Monthly Notices
of the
ROYAL ASTRONOMICAL SOCIETY

MNRAS **489,** 5348–5364 (2019)
Advance Access publication 2019 September 5

doi:10.1093/mnras/stz2457

Dark and luminous satellites of LMC-mass galaxies in the FIRE simulations

Ethan D. Jahn [1]★ Laura V. Sales [1] Andrew Wetzel [2] Michael Boylan-Kolchin [3] T. K. Chan [4] Kareem El-Badry [5] Alexandres Lazar[6] and James S. Bullock[6]

[1]*Department of Physics and Astronomy, University of California Riverside, 900 University Avenue, Riverside, CA 92507, USA*
[2]*Department of Physics, University of California, Davis, CA 95616, USA*
[3]*Department of Astronomy, The University of Texas at Austin, 2515 Speedway Blvd, Stop C1400, Austin, TX 78712, USA*
[4]*Department of Physics, Center for Astrophysics and Space Science, University of California at San Diego, 9500 Gilman Dr., La Jolla, CA 92093, USA*
[5]*Department of Astronomy and Theoretical Astrophysics Center, University of California Berkeley, Berkeley, CA 94720, USA*
[6]*Department of Physics and Astronomy, University of California, Irvine, CA 92697, USA*

Accepted 2019 August 25. Received 2019 August 22; in original form 2019 July 4

ABSTRACT

Within lambda cold dark matter (ΛCDM), dwarf galaxies like the Large Magellanic Cloud (LMC) are expected to host numerous dark matter subhaloes, several of which should host faint dwarf companions. Recent *Gaia* proper motions confirm new members of the LMC system in addition to the previously known SMC, including two classical dwarf galaxies ($M_* > 10^5$ M$_\odot$; Carina and Fornax) as well as several ultrafaint dwarfs (Car2, Car3, Hor1, and Hyd1). We use the Feedback In Realistic Environments (FIRE) simulations to study the dark and luminous (down to ultrafaint masses, $M_* \sim 6\times10^3$ M$_\odot$) substructure population of isolated LMC-mass hosts ($M_{200\rm m} = 1$–3×10^{11} M$_\odot$) and place the *Gaia* + DES results in a cosmological context. By comparing number counts of subhaloes in simulations with and without baryons, we find that, within 0.2 $r_{200\rm m}$, LMC-mass hosts deplete ∼30 per cent of their substructure, significantly lower than the ∼70 per cent of substructure depleted by Milky Way (MW) mass hosts. For our highest resolution runs ($m_{\rm bary} = 880$ M$_\odot$), ∼ 5–10 subhaloes form galaxies with $M_* \geq 10^4$ M$_\odot$, in agreement with the seven observationally inferred pre-infall LMC companions. However, we find steeper simulated luminosity functions than observed, hinting at observation incompleteness at the faint end. The predicted DM content for classical satellites in FIRE agrees with observed estimates for Carina and Fornax, supporting the case for an LMC association. We predict that tidal stripping within the LMC potential lowers the inner dark matter density of ultrafaint companions of the LMC. Thus, in addition to their orbital consistency, the low densities of dwarfs Car2, Hyd1, and Hyd2 reinforce their likelihood of Magellanic association.

Key words: galaxies: dwarf – galaxies: formation – cosmology: dark matter.

1 INTRODUCTION

The lambda cold dark matter (ΛCDM) structure formation scenario predicts a nested hierarchy of dark matter (DM) haloes, subhaloes, and sub-subhaloes at all mass scales from galaxy clusters to well below the molecular cooling limit of 10^6 M$_\odot$ (Press & Schechter 1974; White & Rees 1978; Tegmark et al. 1997; Springel et al. 2008). The abundance of substructure is thought to be nearly scale-free and self-similar. That is, the mass function of subhaloes takes a universal form when normalized to the mass of the host (Gao et al. 2004; Kravtsov et al. 2004; Giocoli, Tormen & van den Bosch 2008; Yang et al. 2011). This means that objects from the most massive haloes at the centres of giant clusters to isolated dwarf galaxies should host a similar distribution of DM substructure when normalized properly.[1] These haloes and subhaloes act as hosts of galaxy formation, providing potential wells in which gas can accumulate and condense into star forming regions. The fact that the relation between stellar mass M_* and halo mass is a near power law below Milky Way (MW) masses (Yang, Mo & van den

★ E-mail: ejahn003@ucr.edu

[1]Though, disruption of subhaloes and galaxies due to baryons complicates this relation, as described later.

© 2019 The Author(s)
Published by Oxford University Press on behalf of the Royal Astronomical Society

Downloaded from https://academic.oup.com/mnras/article-abstract/489/4/5348/5561484 by University of Texas Libraries user on 02 October 2019

Bosch 2003; Behroozi, Conroy & Wechsler 2010; Guo et al. 2010; Moster, Naab & White 2013; Wright et al. 2017), together with the near invariance of subhalo abundance, means that the number of satellite galaxies normalized to the stellar mass of the central is expected to be independent of host halo mass for $\log_{10}(M_*^{\rm host}/{\rm M}_\odot) = 7.25$–$11.75$ (Sales et al. 2013).

The Local Group, consisting of the Milky Way (MW), M31, and their numerous satellite galaxies, offers an ideal testing ground for these ideas. For instance, the Large Magellanic Cloud (LMC), the largest satellite of the MW, has long been speculated to host satellites of its own (Lynden-Bell & Lynden-Bell 1995; D'Onghia & Lake 2008; Sales et al. 2011). Recent observational missions including DES, SMASH, PAN-STARRS, ATLAS, and *Gaia* have revealed numerous dwarf galaxies in the vicinity of the Magellanic system (Bechtol et al. 2015; Drlica-Wagner et al. 2015; Kim & Jerjen 2015; Koposov et al. 2015; Laevens et al. 2015; Torrealba et al. 2016; Gaia Collaboration 2018), greatly expanding the population of potential LMC satellites. Based on the orbital properties of these dwarfs, recent works (Sales et al. 2017; Kallivayalil et al. 2018, hereafter S17 and K18) have discovered several possible associations of dwarf galaxies to the LMC (see also Deason et al. 2015; Jethwa, Erkal & Belokurov 2016; Shao et al. 2018a). According to S17 and K18, there are currently five firm candidates to LMC-system membership: the Small Magellanic Cloud (SMC), Car2, Car3, Hor1, Hyd1, as well as eight promising possible associations awaiting additional proper motion measurements: Dra2, Eri3, Hor2, Hyd2, Phx2, Ret3, Tuc4, and Tuc5. Pardy et al. (2019) have also suggested the possibility of LMC association for the classical dwarf galaxies, Carina and Fornax. We expand on this claim in Section 4. Each new measurement marks a step closer to a complete picture of the pre-infall satellite population of the LMC, which will greatly inform our theories of galaxy formation.

While it is known that satellite galaxies trace substructure, it is unclear from a theoretical perspective exactly how the population of dark subhaloes is mapped to a population of luminous companions. Cosmological *N*-body (dark matter only, 'DMO') simulations (e.g. Navarro, Frenk & White 1996; Jenkins et al. 1998; Springel et al. 2005, 2008) and hydrodynamical baryonic simulations (e.g. Abadi et al. 2003; Governato et al. 2004; Sales et al. 2007; Brooks et al. 2013; Sawala et al. 2016; Wetzel et al. 2016) have been instrumental in making predictions for both central galaxies and smaller scale subhalo and satellite mass functions, as well as in revealing discrepancies between theoretical predictions of dark matter structure and the observed stellar structure that follows it.

Tension in predictions made by numerical simulations with the observed population of galaxies include the 'missing satellites' problem (Klypin et al. 1999; Moore et al. 1999) and 'too big to fail' (Boylan-Kolchin, Bullock & Kaplinghat 2011b; Tollerud, Boylan-Kolchin & Bullock 2014; Kirby et al. 2014; though see also Read et al. 2006; Okamoto & Frenk 2009), which address this mapping from dark to luminous substructure. Encouragingly, several solutions to such problems have been proposed, mostly invoking a combination of reionization heating, observational incompleteness, and the addition of realistic feedback modelling (Bullock, Kravtsov & Weinberg 2000; Somerville 2002; Wang et al. 2015; Wetzel et al. 2016; Sawala et al. 2017; Garrison-Kimmel et al. 2018; Simpson et al. 2018). Furthermore, tides within the host potential affect subhaloes. In particular, the addition of the gravitational potential of the central baryonic disc in MW-mass haloes has been shown to suppress the presence and survival of dark matter subhaloes compared to DMO runs (D'Onghia et al. 2010; Garrison-Kimmel et al. 2017b; Graus et al. 2019). With a smaller population of subhaloes predicted, the number of eligible sites for satellite dwarf galaxies to form is also reduced, highlighting the need for a better understanding of the dark-to-luminous mass mapping predicted within ΛCDM. Because the central galaxy is the source of this effect, the actual efficacy of this effect depends on the M_*–$M_{\rm halo}$ ratio. Galaxies near the size of the MW have the highest M_*–$M_{\rm halo}$ ratio, while galaxies of both higher and lower stellar mass are observed to be hosted by fractionally larger haloes, a trend which motivates exploring the magnitude of subhalo depletion by the central galaxy at different host mass scales.

Many of the above studies do not resolve satellite galaxies down to the scale of ultrafaints (UFs; $M_* \lesssim 10^5$ M$_\odot$) – presumably, the most abundant class of galaxies in our Universe. Since the satellite population of the LMC can be considered a scaled-down version of that of the MW, it is likely to be dominated by UFs, as the current (incomplete) population of LMC satellites seems to suggest. Due to their shallower gravitational potential, the effects of reionization at this scale of galaxy formation are believed to be stronger than for more massive galaxies like the MW or classical dwarf spheroidals (though feedback effects are weaker since they form proportionally fewer stars). Thus, exploring the UF population of the LMC (and of LMC-mass hosts in general) is critically important to push the limits of our knowledge of dark-to-luminous substructure mapping into much fainter scales than currently known.

A possible avenue to overcome numerical resolution limitations in cosmological simulations is to focus on the formation of isolated dwarf galaxies. The lower masses and smaller sizes expected for dwarf haloes translate into smaller mass per particle and smaller gravitational softening at a fixed number of particles compared to a more massive halo. For example, Wheeler et al. (2015, 2018) were able to study an extremely high-resolution population of UF satellites in simulations of dwarf host haloes in the scale $M_{\rm 200m} \sim 10^{10}$ M$_\odot$. On average, 1–2 UFs were expected above $M_* \geq 3 \times 10^3$ M$_\odot$, making important predictions for the numbers and distribution of UF dwarfs around dwarf galaxies in the field. Promisingly, larger numbers of UFs shall be expected for more massive dwarf hosts. The inferred virial mass of the LMC, $\sim 10^{11}$ M$_\odot$ at the large end of the dwarf galaxy scale, promises to provide numerous substructures with which subhalo abundance can be studied. In addition, its recent infall to the MW (1–3 Gyr ago, Kallivayalil et al. 2013), means its satellite population will remain relatively undisturbed by the tidal field of the MW (Sales et al. 2011; Boylan-Kolchin, Besla & Hernquist 2011a; Deason et al. 2015) and may offer an observational avenue to reconstruct its pre-infall satellite companions.

Previous theoretical works on Local Group satellite galaxies have predicted that ∼30 per cent of $M_* \lesssim 10^5$ M$_\odot$ satellites of MW-mass hosts fell in as a satellite of a more massive galaxy (Wetzel, Deason & Garrison-Kimmel 2015), and that such groups of dwarf galaxies typically disperse in phase space about 5 Gyr after infall to an MW/M31 system (Deason et al. 2015). In addition, Dooley et al. (2017) predicts ∼8 large UF dwarf satellites of the LMC using reionization and abundance matching models with the Caterpillar simulations (Griffen et al. 2016). However, such predictions are all based on DMO simulations missing important phenomena expected once the baryons are self-consistently taken into account, for example, SNe feedback, gas hydrodynamics affecting morphology, and tidal effects from the central baryonic disc.

In this work, we present the first analysis of satellite galaxies down to the UF mass scale in simulations of LMC-mass hosts, using the Feedback In Realistic Environments (FIRE) project. We investigate the luminous and dark substructure of these hosts in hope of gleaning insight into the real history of the LMC system.

Downloaded from https://academic.oup.com/mnras/article-abstract/489/4/5348/5561484 by University of Texas Libraries user on 02 October 2019

How many satellites, dark and luminous, did the LMC bring with it as it fell into the MW system? What is the mass distribution of these satellites? How have they been shaped by co-evolution with the LMC, and does this differ from satellites/substructures of the MW? Are there ways of constraining membership beyond orbital phase space having similarity with the LMC?

Previous works using the FIRE simulations have shown promising results, making them a compelling laboratory to investigate these questions. Recent relevant work includes the observational agreement in classical satellites of MW-mass hosts (Wetzel et al. 2016; Garrison-Kimmel et al. 2018), the star formation histories of satellite galaxies in various Local Group inspired environments (Garrison-Kimmel et al. 2019), radial profiles of classical satellites (Samuel et al. 2019), the origin and evolution of the mass–metallicity relation (Ma et al. 2016), chemical abundance distribution of dwarf galaxies (Escala et al. 2018), as well as gas kinematics and morphologies in dwarf galaxies (El-Badry et al. 2018a,b).

This paper is organized as follows: In Section 2, we descibe the FIRE simulations, including the feedback model, the zoom-in technique, halo finding, and resolution. We also describe our sample of LMC-mass zoom-in runs. In Section 3, we describe the effect of the central galaxy population of the abundance of subhaloes as compared to DMO runs. In Section 4, we expand on the analysis of S17, K18, and Pardy et al. (2019) by analysing *Gaia* orbital angular momenta of satellites in Gaia Collaboration (2018). We compare the updated observationally inferred pre-infall mass function of the LMC to the satellite populations in our FIRE runs. We also investigate the structural kinematics of both observed and simulated dwarf satellites, with a focus on UF dSphs, and consideration of infall time and tidal stripping. We present a summary of this work and concluding remarks in Section 5.

2 SIMULATIONS

We analyse a sample of five cosmological zoom-in simulations of LMC-mass host galaxy systems from the Feedback In Realistic Environments (FIRE) project.[2] These runs, implemented in the updated FIRE-2 scheme (Hopkins et al. 2018b), use the fully conservative cosmological hydrodynamic code GIZMO[3] (Hopkins 2015), a multimethod gravity plus hydrodynamics code, in its meshless finite-mass mode. This is a mesh-free Lagrangian finite-volume Godunov method, which automatically provides adaptive spatial resolution while maintaining conservation of mass, energy, and momentum, and excellent shock-capturing and conservation of angular momentum, capturing advantages of both smoothed-particle hydrodynamics and Eulerian adaptive mesh refinement schemes (for extensive tests, see Hopkins 2015). Gravity is solved with an improved version of the Tree-PM solver from GADGET-3 (Springel 2005), with fully adaptive (and fully conservative) gravitational force softenings for gas (so hydrodynamic and force softenings are always self-consistently matched), following Price & Monaghan (2007).

FIRE-2 implements a variety of methods for cooling, star formation, and stellar feedback processes. Heating and cooling rates are calculated across 10–10^{10} K, including CLOUDY ionization states for free–free, photoionization and recombination, Compton scattering, photoelectric, metal-line, molecular, fine structure, dust collisional, uniform cosmic ray heating, from a spatially uniform, redshift-dependent UV background (Faucher-Giguère et al. 2009). Local self-shielding is accounted for using a Sobolev approximation. Stars are formed in accordance with Hopkins, Narayanan & Murray (2013), requiring gas to be locally self-gravitating, self-shielding (following Krumholz & Gnedin 2011), Jeans unstable, and with density $n_{\rm H} > n_{\rm crit} = 1000$ cm^{-3}, with all conditions met. Global star formation efficiency is naturally self-regulated by feedback processes, with good observational agreement (Orr et al. 2018). All newly formed star particles inherit mass and metallicity from their progenitor gas particles.

Stellar feedback quantities are tabulated from the stellar population model STARBUST99 (Leitherer et al. 1999), assuming a Kroupa (2001) IMF, including supernova Type Ia, II, and stellar winds, as detailed in Hopkins et al. (2018a, 2018b). Radiative feedback is modelled with the Locally Extincted Background Radiation in Optically thin Networks (LEBRON) algorithm (Hopkins et al. 2018b), accounting for absorbed photon momentum, photoionization, and photoelectric heating.

The zoom-in technique (Katz & White 1993; Oñorbe et al. 2015) is implemented by first simulating a large, low-resolution cosmological box in which a convex Lagrangian region (at initial redshift) is then defined. The region contains all particles within $\sim 5 r_{\rm vir}$ at $z = 0$ and *not* containing a halo of similar mass to that of the primary, and is then reinitialized with higher resolution. This process is repeated to refine the Lagrangian region until the intended resolution is reached, at which point it is re-simulated with dark matter, gas, and star particles, buffered by a region of lower resolution dark matter particles. Initial conditions[4] are generated with the MUSIC code (Hahn & Abel 2011), which implements a second-order Lagrangian perturbation theory to $z = 99$.

Structure and substructure are identified using an updated version of the ROCKSTAR halo finder (Behroozi, Wechsler & Wu 2013a), which implements 6 + 1 dimensional phase-space analysis to determine the particles that are gravitationally bound and assign them to (sub)haloes. ROCKSTAR assigns mass to haloes and subhaloes using spherical overdensity calculations relative to a specified threshold, such as the critical density or the average matter density of the Universe. Such quantities necessarily become ambiguous and unreliable when quantifying masses of substructure, because the mass density of such embedded objects is by definition above the chosen threshold. To circumvent this ambiguity, we will mostly refer to the maximum circular velocity as an analog for subhalo mass, because it is a more robust and well-defined metric. For numerical stability, we run ROCKSTAR using only dark-matter particles, and we assign star particles in post-processing using an iterative procedure. We first select star particles within a DM halo out to 0.8 $r_{\rm halo}$ and with velocities less than 2 $V_{\rm max}$ of the (sub)halo's centre of mass velocity, and we iteratively compute stellar position and velocity (making sure the star particles and halo are coincident) until the total mass of star particles, M_*, converges to <1 per cent. See Samuel et al. (2019) for a more detailed description.

2.1 Resolution convergence

All simulations analysed herein contain no low-resolution particles within $\sim 3\ r_{\rm 200m}$ from the host centre. However, the 7070 $M_\odot$ resolution runs naturally use fewer particles to represent objects at a given mass than do the higher resolution runs, leading to

[2] http://fire.northwestern.edu
[3] http://www.tapir.caltech.edu/ phopkins/Site/GIZMO.html
[4] http://www.tapir.caltech.edu/ phopkins/publicICs/

Downloaded from https://academic.oup.com/mnras/article-abstract/489/4/5348/5561484 by University of Texas Libraries user on 02 October 2019

Table 1. Properties of the host halo of all simulations analysed herein for both the *N*-body DMO run (`-dmo`) and hydrodynamic run (no suffix) at $z = 0$. References for additional details on each simulation are shown in the rightmost column. Our primary sample, the LMC-mass `m11` hosts, are shown in the top block, and our reference sample, the MW-mass `m12` hosts, are shown below. Resolution refers to the baryonic mass resolution. All quantities are computed from halo catalogues generated by the ROCKSTAR halo finder (calculated using DM particles unless the item explicitly refers to stellar quantities, e.g. M_*). The minimum $V_{\rm max}$ is the median value for subhaloes of $195 < N_{\rm particles} < 205$, and serves as an effective resolution limit for substructures in each simulation. This particle number was chosen in accordance with the Hopkins et al. (2018b) determination of DM convergence radii with the Power et al. (2003) criterion. The virial radius ($r_{\rm 200m}$) is the radius where the average interior DM density is equal to 200 times the mean matter density in the Universe. The number of subhaloes within $0.2\times r_{\rm 200m}$, $0.4\times r_{\rm 200m}$, and $r_{\rm 200m}$ of the host are selected as having $V_{\rm max} > 5$ km s^{-1}, this cut-off value is chosen to include only confidently resolved subhaloes in all simulations. Note that `m11c` and `m11v` do not have DMO versions. In the last column, we include the number of luminous satellites, defined as $M_* > 0$, though, practically, the stellar mass of the smallest resolved satellite (and hence total number of resolved satellites) varies with resolution. All $M_{\rm 200m}$ and M_* for non-DMO `m12` simulations were taken from Samuel et al. (2019), as they include all mass components in the calculation of $M_{\rm 200m}$, as well as only include stellar mass associated with the galactic disc (i.e. excluding stellar mass contained in the stellar halo).

Simu-lationlation	Resolution ($M_\odot$)	$M_{\rm 200m}$ ($M_\odot$)	M_* ($M_\odot$)	$r_{\rm 200m}$ (kpc)	$V_{\rm max}$ (km s^{-1})	min. $V_{\rm max}$ (km s^{-1})	$N_{\rm sub}$ $< 0.2r_{\rm 200m}$	$N_{\rm sub}$ $< 0.4r_{\rm 200m}$	$N_{\rm sub}$ $< r_{\rm 200m}$	$N_{\rm lum}$ $< r_{\rm 200m}$	Ref.
`m11c`	2100	1.5e11	8.2e8	167.4	81.0	2.5	9	34	118	9	1
`m11d`	7070	2.8e11	4.1e9	203.9	88.8	4.0	16	76	257	11	2
`m11d-dmo`	7070	3.4e11		216.5	95.4	4.8	21	95	333		3
`m11e`	7070	1.5e11	1.4e9	166.0	84.3	4.2	10	31	129	5	2
`m11e-dmo`	7070	1.8e11		176.2	92.1	4.6	4	34	162		3
`m11q`	880	1.5e11	3.4e8	168.7	81.0	1.7	17	56	123	8	4
`m11q-dmo`	880	1.9e11		182.5	91.2	1.8	20	81	192		4
`m11v`	7070	2.9e11	2.4e9	210.5	84.0	4.0	11	62	257	6	4
`m12b`	7070	1.4e12	7.3e10	335.1	180.9	4.2	19	125	544	25	5
`m12b-dmo`	7070	1.4e12		358.8	178.8	4.7	91	343	1116		5
`m12c`	7070	1.4e12	5.1e10	328.4	156.4	4.0	62	285	895	42	5
`m12c-dmo`	7070	1.3e12		350.0	154.1	4.4	156	537	1492		5
`m12f`	7070	1.7e12	6.9e10	354.7	183.4	4.0	34	202	863	31	4,5
`m12f-dmo`	7070	1.8e12		383.7	176.0	4.6	132	519	1693		4,5
`m12i`	7070	1.2e12	5.5e10	314.2	161.2	4.0	28	194	681	24	4,5
`m12i-dmo`	7070	1.2e12		339.3	162.3	4.8	103	431	1225		4,5
`m12m`	7070	1.6e12	1.0e11	341.6	184.3	4.3	48	259	900	40	4,5
`m12m-dmo`	7070	1.5e12		364.5	171.1	4.9	116	515	1622		4,5
`m12r`	7070	1.1e12	1.5e10	304.3	136.8	4.1	53	250	822	28	6
`m12r-dmo`	7070	1.1e12		322.6	146.0	4.8	95	420	1192		6
`m12w`	7070	1.1e12	4.8e10	300.5	156.2	4.5	33	181	638	31	6
`m12w-dmo`	7070	1.2e12		328.3	158.6	4.9	125	448	1167		6

Note: References: 1 -– Chan et al. (2018); 2 – El-Badry et al. (2018a); 3 – Lazar et al. (in preparation); 4 – Hopkins et al. (2018b); 5 – Wetzel et al. (2016); 6 – Samuel et al. (2019).

convergence issues. For this reason, we have determined a minimum value for $V_{\rm max}$, above which subhaloes have $\gtrsim$200 DM particles, as listed in Table 1. We make this cut for all subhaloes analysed herein, and all galaxies naturally fall above this threshold. Using two different resolution runs of `m11q` (7070 and 880 $M_\odot$), we found that the subhalo populations deviate around $V_{\rm max} \sim 4$ km s^{-1}, which is below our cut-off in $V_{\rm max}$. This is shown in Fig. A1.

2.2 Our sample: LMC-like centrals and dark matter cores

Our centrals are selected in the halo mass range $M_{\rm 200m} = 1.5{-}3.4\times10^{11}$ $M_\odot$, where $M_{\rm 200m}$ refers to the mass measured within $r_{\rm 200m}$, defined as the radius at which the mean interior halo density equals 200 times the average matter density of the Universe. The stellar masses of the centrals at $z = 0$ are in the range $M_* = 0.34{-}4.1\times10^9$ $M_\odot$, compared to the 1.5×10^9 $M_\odot$ of the LMC (McConnachie 2012). These and other properties of our centrals are listed in Table 1. Our choice of '200m' (as opposed to '200c' which uses the critical density of the Universe, $\rho_{\rm crit}$) is motivated by its closer physical proximity to the 'splashback' radius, in which all (dark) matter that has passed through the core of the halo is enclosed (see Wetzel & Nagai 2015, Section 2, for a detailed explanation).

We analyse the highest resolution runs available for each system. There are three 'low'-resolution ($m_{\rm bary} = 7070$ $M_\odot$) runs: `m11c`, `m11d`, `m11e`; one medium-resolution run ($m_{\rm bary} = 2100$ $M_\odot$): `m11c`; and one high-resolution run ($m_{\rm bary} = 880$ $M_\odot$): `m11q`. For the first part of this analysis, we consider `m11d`, `m11e`, and `m11q` to be our primary focus because they have counterpart DMO simulations, allowing a comparative analysis of subhalo populations between DMO and baryonic versions of the same system. We examine all runs in Section 4, where we investigate the population of luminous companions around each host. All simulations were run with the core the FIRE-2 hydrodynamics and feedback models, while `m11q`, `m11d`, and `m11e` implemented an additional subgrid model for the turbulent diffusion of metals in gas. By comparing `m11q` with and without this model, we have observed no difference in the mass and abundance of satellite galaxies, in agreement with Hopkins et al. (2018b) and Su et al. (2017), which quantified that including (or not including) metal diffusion physics did not change galaxy-wide properties. Phenomena sensitive to the physics of metal diffusion (such as metallicity gradients) are beyond the scope of this paper, so we proceed considering all runs equivalently.

To showcase our sample, the top panels in Fig. 1 show a visualization of the baryons (left) and the dark matter (right) within a region slightly larger than the virial radius of our highest resolution halo `m11q`. The dark matter component shows a large number of subhaloes as expected within ΛCDM. On the left, stars (yellow) and gas (blue) have collapsed at the centre of this LMC-mass

Downloaded from https://academic.oup.com/mnras/article-abstract/489/4/5348/5561484 by University of Texas Libraries user on 02 October 2019

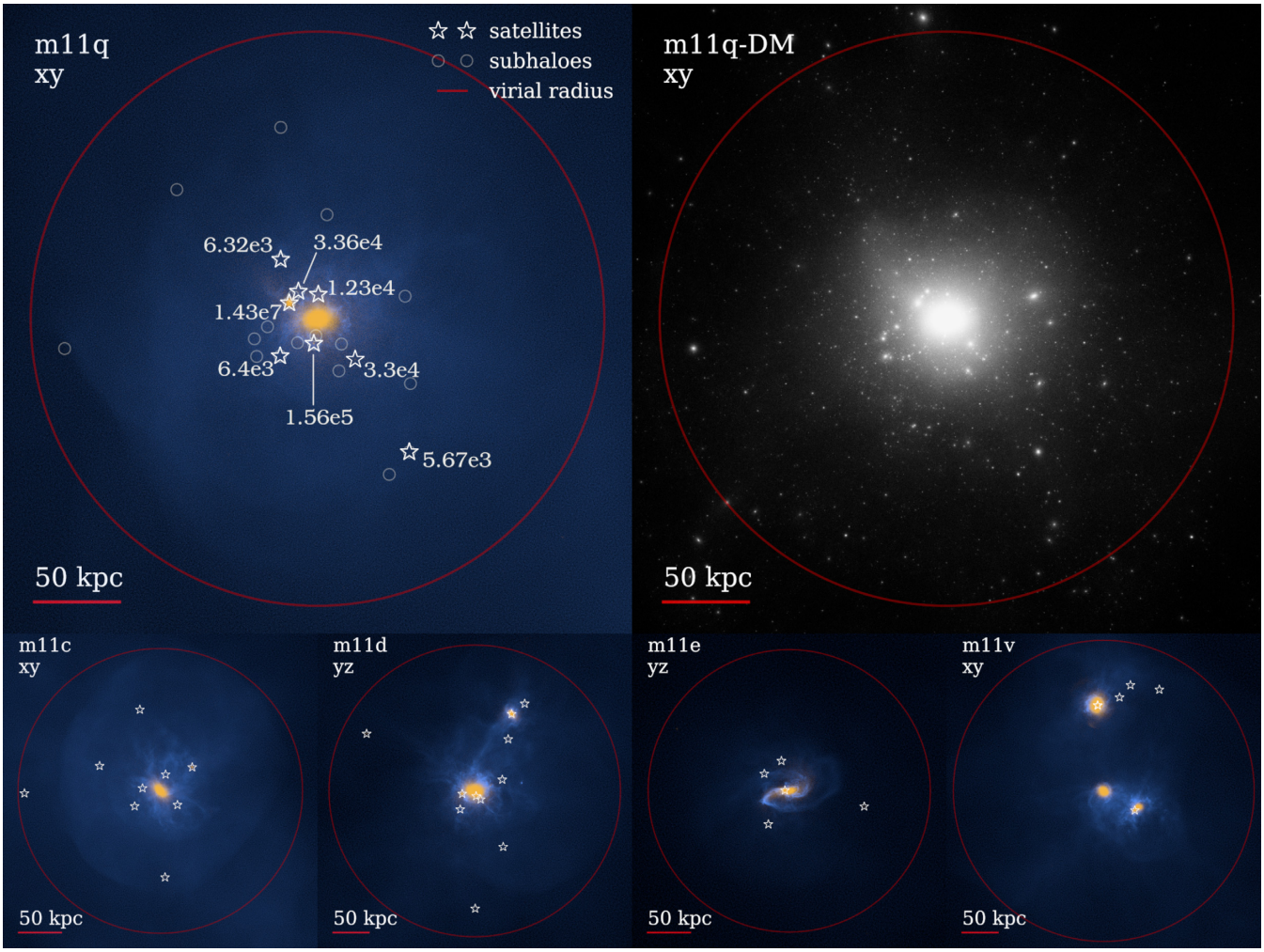

Figure 1. Projections of our sample of LMC-analogue host galaxies in FIRE, with the virial radius (r_{200m}) of each host shown as a red circle. The top left panel shows a detailed projection of the highest resolution run, `m11q`, with stars in yellow and gas in blue. The 15 subhaloes of highest V_{max} (down to 9.6 km s^{-1}) are shown by grey circles, chosen only to give a visually representative sample of subhaloes. All satellite galaxies are shown by grey star markers, with their stellar mass in solar masses ($M_\odot$) shown nearby. The dark matter content of the same simulation is shown in the top right panel – a few direct comparisons can be made between bright spots here and subhalo markers on the left. The bottom four panels show the stars and gas of `m11c`, `m11d`, `m11e`, and `m11v` with satellite galaxies located by star markers. All of our hosts are isolated in the sense that they are not within the realm of influence of a larger halo, such as the Milky Way. However, `m11v` is an ongoing multimerger, with two neighbours of stellar and virial masses $\lesssim$ that of the host. All other runs are unambiguously isolated.

halo to form the central dwarf, with $M_* \sim 3\times10^8$ M$_\odot$. However, several other satellite subhaloes have also formed stars giving rise to the population of dwarf satellites. We highlight them with starred symbols and annotate their corresponding stellar masses. The dark-to-luminous mapping at these low masses is complex, with only a few subhaloes forming stars and the rest remaining dark companions. Circles on the left panel indicate the fifteen subhaloes of highest V_{max} that have remained dark. The bottom row shows stars and gas for the rest of our sample and nicely illustrates the variations expected on the luminous companions of the LMC-mass haloes.

Table 1 lists relevant properties of the LMC-analogues analysed herein. Also listed, for comparison, is the Latte suite of isolated MW-mass hosts (see e.g. Wetzel et al. 2016; Garrison-Kimmel et al. 2017b, hereafter GK17). See Section 2.3 for more details on these simulations. The selection of all LMC-like hosts was blind with respect to satellite and subhalo population, aside from `m11v`, which was selected to have an ongoing merger at $z = 0$, as can be seen by its two companions, each with $M_* \gtrsim M_*$(SMC) $\sim 4\times10^8$ M$_\odot$. All were selected to be isolated from larger haloes within $\sim$5 r_{200m}.

At $z = 0$, our LMC-mass centrals all show a cored dark matter density profile (see left-hand panel of Fig. 2) which contrasts with the denser and cuspy nature of the DMO runs (shown for haloes `m11q`, `m11d`, and `m11e` in dashed lines). This is better indicated in the bottom panel showing the ratio between the dark matter density in the DMO run to the baryonic run, ρ_{dmo} / ρ_{hydro}, as a function of radius. Our LMC-mass centrals show 3–10 times lower densities in the inner regions when the effect of baryons is included, an effect that is much larger than that observed in more massive M_{200m} $\sim 10^{12}$ M$_\odot$ hosts run with similar feedback[5] (dot–dashed purple line showing results from Latte, e.g. Wetzel et al. 2016; Lazar et al., in preparation).

[5] `m11d` and `m11e` are in the final stages of a merger at $z = 0$, making their cores seem larger due to the poorly defined centre of each halo.

Downloaded from https://academic.oup.com/mnras/article-abstract/489/4/5348/5561484 by University of Texas Libraries user on 02 October 2019

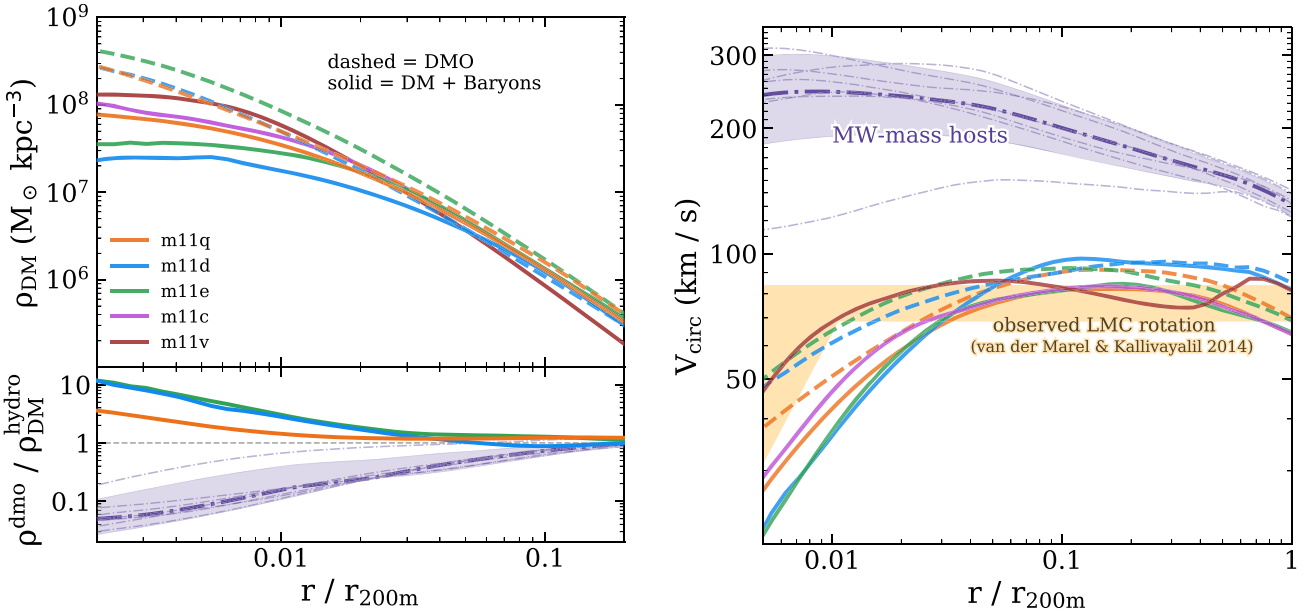

Figure 2. (Left) The top panel shows the DM density of FIRE LMC-mass hosts with distances normalized to r_{200m}. DMO runs are shown as dashed lines while the total mass density for the Hydro runs are shown as solid lines. The bottom panel shows the DMO-to-Hydro density ratio, which quantifies the degree of coring. This is shown for MW-mass hosts as the purple dashed–dot line, shaded for the 1σ deviation from the mean at $z = 0$. All `m11` runs are heavily cored in comparison to the MW-mass hosts. (Right) Circular velocity profiles of all hosts. V_{circ} for baryonic runs is calculated using total mass (DM + stars + gas). The observed circular velocity of the LMC is shaded in orange, representing a 1σ interval from a parametrized fit of proper motion measurements (van der Marel & Kallivayalil 2014). We find good agreement with our simulated LMC-mass hosts for $r/r_{200m} \gtrsim 0.04$, though all but `m11v` have somewhat lower circular velocities in the inner regions.

The formation of cores in our LMC-like galaxies responds to the rapid removal of self-gravitating gas at the centre of the halo due mainly to supernova explosions, which changes temporarily the potential at the centre of the haloes and leads to the 'heat up' of the orbits of dark matter particles (Navarro et al. 1996; Peñarrubia et al. 2010; Pontzen & Governato 2012; Garrison-Kimmel et al. 2014). This is consistent with the starbursty nature of star formation reported in FIRE simulations (Chan et al. 2015; Oñorbe et al. 2015; El-Badry et al. 2016; Fitts et al. 2017) and also coincides with the regime where core formation due to the effect of baryons is expected to be maximal (Di Cintio et al. 2014; Chan et al. 2015; Tollet et al. 2016). However, El-Badry et al. (2017) showed that the degree of coring is subject to change on relatively short time-scales as gas outflows and inflows change. This mass rearrangement also affects the circular velocity profiles, as shown by the right-hand panel of Fig. 2. Considering the effects of baryons, the maximum circular velocities of our haloes are on the high end of agreement with that measured from *HST* proper motions of stars in the LMC (indicated by the orange shaded region van der Marel & Kallivayalil 2014).

2.3 Our sample: MW-mass centrals

To highlight the dependence on host mass of many phenomena explored herein, we compare to the Latte suite of seven zoom-in simulations of MW-mass hosts (`m12b`, `m12c`, `m12f`, `m12i`, `m12m`, `m12r`, and `m12w`; introduced in Wetzel et al. 2016) with both baryonic and DMO runs, all with a baryonic mass resolution of 7070 $M_\odot$. All MW-mass hosts were blindly selected, with the exception of `m12r` and `m12w`, which were chosen to have an LMC-mass satellite at $z = 0$ in DMO (although, the LMC companion does not necessarily survive to $z = 0$ in the baryonic runs, see Samuel et al. 2019). These simulations confidently resolve subhaloes down to $V_{max} \sim 4$ km s^{-1}, and luminous satellite galaxies down to $M_* \sim 1\times10^5$ $M_\odot$ (galaxies with $M_* < 1\times10^5$ $M_\odot$ are mostly found in the higher resolution runs). Halo masses range from 1.1×10^{12} to 1.7×10^{12} $M_\odot$, while stellar masses range from 1.5×10^{12} to 10×10^{10} $M_\odot$. The mean stellar mass to halo mass ratio is $\sim 6\times10^{-2}$, compared to $\sim 8\times10^{-3}$ for the LMC-mass hosts. As shown in Fig. 2, the central densities of the MW-mass hosts are much greater than those of our LMC-mass hosts, likely due to the effects of baryonic contraction (Chan et al. 2015). This difference in host density is highly relevant to the discussion on subhalo abundances in the following section.

Any references to the names of various simulations are references specifically to the host/central galaxy of that simulation. The term 'companion' refers to a galaxy of non-zero stellar mass within r_{200m} of its host, while 'subhalo' refers to the self-bound dark matter content of any object – luminous or dark – also within r_{200m} of its host. 'Satellite' is a collective term for either. As it is a common phrase, we also use the term 'virial radius' to refer to r_{200m}, and 'virial mass' for M_{200m}. Note that we do not use the Bryan & Norman (1998) formulation for virial quantities.

3 SUPPRESSION OF DARK MATTER SUBHALOES IN LMC-LIKE HOSTS

The number of subhaloes above a given V_{max}, referred to as the V_{max} function, is a useful metric to evaluate the abundance and scale of substructure hosted by a central halo. In the last decade, it has been found that the V_{max} function in MW-mass haloes may be significantly suppressed when considering the increased tidal disruption due to the effect of the baryons in the central disc (D'Onghia et al. 2010; Kelley et al. 2019, GK17). The lower number of surviving subhaloes results in a different prediction of

Downloaded from https://academic.oup.com/mnras/article-abstract/489/4/5348/5561484 by University of Texas Libraries user on 02 October 2019

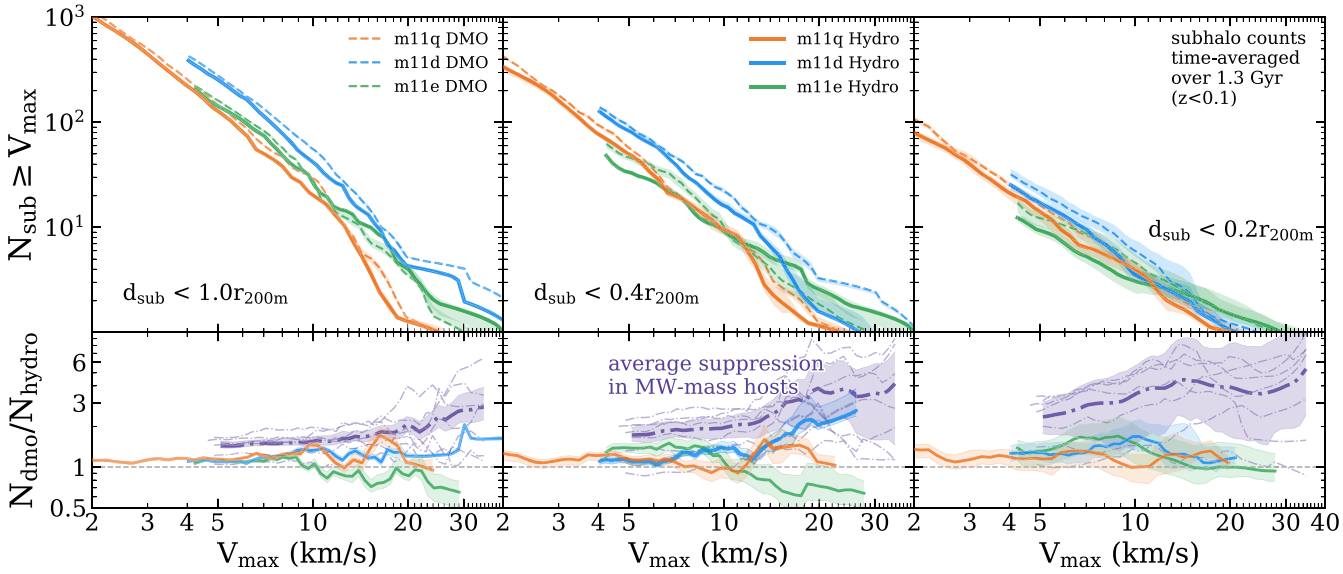

Figure 3. Cumulative time-averaged subhalo count above a given V_{max} within r_{200m} (left), 0.4 r_{200m} (centre), and 0.2 r_{200m} (right) of the host. Counts are averaged over the last ∼1.3 Gyr (z<0.1) to account for fluctuations in subhalo counts as they pass in and out of each cut-off radius. Each line only extends down to the minimum V_{max} as listed in Table 1, and shaded regions indicate 1σ deviation from the mean count at a given V_{max}. Subhalo V_{max} in DMO simulations are normalized by $\sqrt{1-f_b}$ to achieve a one-to-one comparison. The bottom panels quantify the magnitude of subhalo depletion as the ratio of the number of subhaloes at each V_{max} in DMO to Hydro. The grey dotted line at $N_{dmo}/N_{hydro} = 1$ represents no depletion (subhalo populations are equivalent in both runs). The purple dashed lines on the bottom panel show the time-averaged depletion of subhaloes in MW-mass haloes at the corresponding fraction of r_{200m} for each host. We observe weaker depletion in the LMC-mass haloes as compared to the MW mass haloes, consistent with a cored potential and lower stellar mass fraction. Table 2 shows the average amount of depletion for subhaloes of $V_{max} = 10\,km\,s^{-1}$ for the radial cut-offs made here, for both LMC-mass and MW-mass hosts.

Table 2. Average subhalo depletion (N_{dmo}/N_{hydro}) at $V_{max} = 10\,km\,s^{-1}$ for both MW-mass hosts ($M_{halo} \sim 10^{12}$ $M_\odot$) and LMC-mass hosts ($M_{halo} \sim 10^{11}$ $M_\odot$). Each column specifies the cut-off distance inside which subhaloes are counted. Among LMC-mass hosts, we observe modest depletion ($N_{dmo}/N_{hydro} \approx$ 1.1–1.4) of subhaloes at all radii, while subhalo depletion is a strong function of distance for MW-mass hosts.

d_{sub} <	N_{dmo}/N_{hydro} r_{200m}	N_{dmo}/N_{hydro} 0.4 r_{200m}	N_{dmo}/N_{hydro} 0.2 r_{200m}
MW-mass	1.54 ± 0.06	$1.98^{+0.28}_{-0.22}$	$3.51^{+1.82}_{-1.72}$
LMC-mass	$1.28^{+0.12}_{-0.1}$	$1.14^{+0.35}_{-0.23}$	$1.39^{+0.79}_{-0.58}$

the expected number of dwarfs around the MW and in particular for the inner regions where the suppression is maximal. This effect is critical for accurately predicting the radial distribution of satellites around the MW and M31 (Samuel et al. 2019). These and many other recent studies have primarily been concerned with massive host haloes such as the MW. In this section we extend the scope of such inquiry to LMC-mass centrals, with a focus on the suppressing effect of the central baryonic galaxy, by comparing subhalo populations in DMO simulations to subhalo populations of the same centrals simulated with hydrodynamics & baryonic physics.

Fig. 3 shows the time-averaged subhalo V_{max} function of three LMC-mass hosts (orange – `m11q`; blue – `m11d`; green – `m11e`) as a cumulative count of subhaloes at a given V_{max} and within different radial cuts from r_{200m} to 0.2 r_{200m} (left to right). Subhaloes in each run are plotted from the highest V_{max} present to the minimum converged V_{max}, as listed in Table 1. Time-averaging was computed over the most recent ∼1.3 Gyr, or $z \lesssim 0.1$ by sampling the V_{max} function of every host at each successive snapshot (66 in total), then computing the mean number of subhaloes at each V_{max}, including the 1σ deviation from the mean (shaded regions). Shading for the average depletion among the Latte suite of MW-mass simulations (bottom panels, purple dash–dotted lines) was calculated by adding the 1σ deviations in quadrature, for each run at each V_{max}. Within the virial radius of a $M_{200m} \sim 10^{11}$ $M_\odot$ halo, on average one can expect order 10 subhaloes with $V_{max} \geq 10\,km\,s^{-1}$ and order 10^2 above $5\,km\,s^{-1}$. We have explicitly checked that the radial distribution of those subhaloes follows closely that of the dark matter in the host.

We additionally include the DMO subhalo populations of all hosts to illustrate how the additional baryonic potential and feedback effects change the distribution and total number of subhaloes. This difference is quantified in the bottom panel where the number of subhaloes at a given V_{max} in DMO is divided by that number in Hydro. A number greater than one represents 'suppression' or 'depletion' of subhaloes in the Hydro run, while a number less than one means there are more subhaloes at that V_{max} in Hydro than in DMO, or an 'enhancement' of substructure.

A close inspection of the bottom row in Fig. 3 shows that, on average, all subhaloes with $V_{max} < 15\,km\,s^{-1}$ are only slightly suppressed (by a factor of ∼ 1.3) in hydro runs compared to the DMO version, an effect that increases only mildly when looking into the inner regions (middle and right panels). While time-averaging is indeed implemented to mitigate the discreteness of the sample, there are not many (<10) satellites with $V_{max} > 15\,km\,s^{-1}$ around LMC-like hosts and Poisson fluctuation may dominate. Take, for example, halo `m11e` (green). Although the middle panel seems to suggest an increase in the number of subhaloes in the hydro run with respect to the DMO, the effect seems localized and it disappears for the inner regions ($r < 0.2\,r_{200m}$, right-hand panel). We interpret this as a local fluctuation that results from poor numbers statistics: only six subhaloes exist with $V_{max} = 10\,km\,s^{-1}$. We see that the overall

Downloaded from https://academic.oup.com/mnras/article-abstract/489/4/5348/5561484 by University of Texas Libraries user on 02 October 2019

trend in our LMC-mass hosts is a mild to negligible suppression of their subhalo populations by their central galaxies.

Also included in the bottom panel is the average suppression of subhaloes for all MW-mass Latte hosts within the same fraction of their virial radii as our LMC-mass haloes (see also GK17; Samuel et al. 2019). In all panels we find that the level of suppression in our LMC-mass haloes is significantly smaller than in MW-mass haloes. This is most evident in the inner regions $r < 0.2\,r_{200m}$, where subhaloes are depleted by a factor $\sim$ 3–6 in the `m12`'s compared to a maximum of $\lesssim 1.5$ in our best resolved (though least cored) halo `m11q`. These results are mostly independent of the simulation method used. For example, using DMO runs with an added analytic disc D'Onghia et al. (2010) show that MW-mass environments suppress subhaloes by a factor ~ 3 at 10^7 M$_\odot$ (V_{max}= 4–5 km s^{-1}) within 30 kpc of the centre, compared to at most a factor 2 found in our LMC-mass environments. The lower impact of baryons on the number of subhaloes for LMC-mass hosts is consistent with previous arguments. Using hydrodynamical simulations and comparing to an analytic disc potential, GK17 showed that the primary mechanism for suppression of substructure is the enhanced tidal stripping of subhaloes by the gravitational potential of the central galaxy. This is due to two effects in the scale of MW-mass hosts. First, the extra component added to the gravitational forces by the presence of the disc and, secondly, by the dark matter halo itself becoming more concentrated in the presence of the disc leading to a steeper gravitational potential well.

We note that we find no correlation between substructure depletion and resolution. For instance, Fig. 3 shows that 'normal' resolution (`m11d` and `m11e`) can show either more or less substructure depletion than the high resolution run `m11q`. There is therefore not an obvious systematic effect with resolution. Instead, substructure depletion may depend on the specifics of the central baryonic mass and accretion history of each halo. This is consistent with the lack of dependence in the resolution tests for N_{dmo}/N_{hydro} in MW-mass hosts as examined in GK17 and Samuel et al. (2019).

In the case of hosts within the $M_{200m} = 10^{11}$ M$_\odot$ regime, as analysed here, the fraction of mass in the disc is much smaller than in MW-mass objects ($\sim$1 per cent average for the LMC-analogues compared to $\sim$6 per cent for the MW-analogues) partially explaining the lower suppression of substructure. Additionally, the dark matter haloes of LMC-hosts in Hydro are predicted to be less dense compared to their DMO counterparts (see Fig. 2) due to the effect of stellar feedback; opposite to the trend found in MW-mass hosts, which are dominated by baryonic contraction. We conclude that substructure depletion is less significant in dwarfs centrals than expected in $\sim L_*$ galaxies and that hundreds of dark matter subhaloes with $V_{max} > 5$ km s^{-1} are expected to be orbiting around field dwarf galaxies with mass comparable to the LMC.

3.1 Implications for observational subhalo searches

Constraining the degree of subhalo suppression in regions near galaxies has strong implications on the viability of observational subhalo searches that are based on gaps in cold stellar streams. As noted by GK17, if all subhaloes within 20 kpc of the MW are suppressed by the baryonic disk, it is less likely for surveys like Palomar-5 and GD-1 (Koposov, Rix & Hogg 2010; Carlberg, Grillmair & Hetherington 2012) to detect any interaction with cold dark matter substructure [see also Chapman et al. (in preparation), who detected a non-trivial infall rate of subhaloes into the inner regions of FIRE MW-mass hosts, but that those subhaloes are quickly destroyed]. By examining the $z = 0$ radial distribution of substructures with $V_{max} > 10$ km s^{-1} as seen in Fig. A3, we find that, on average, the MW-mass haloes host no substructure within 30 kpc (though individual haloes may occasionally have a few subhaloes in the range 20 kpc $< d_{sub} <$ 30 kpc). On average, the LMC-mass haloes are able to host substructure down to $\sim$20 kpc, while retaining roughly a factor of two more subhaloes than MW-mass hosts up to approximately 45 kpc. The total number of subhaloes hosted by MW-mass haloes only surpasses that of LMC-mass haloes at $\sim$60–70 kpc. In addition, the overall reduced effect of host-subhalo tidal interactions make LMC-mass hosts somewhat cleaner systems to study substructure than their more strongly interacting MW-mass counterparts. We therefore argue that the study of cold streams around galaxies with $M_* \sim 10^9$ M$_\odot$ may represent a more promising avenue to detect gaps associated with these dark subhaloes.

Of course, the mass range of the substructure is also important. Previous work quantifying the sensitivity of cold stellar structures to disturbances by subhaloes (e.g. Yoon, Johnston & Hogg 2011) suggest that streams such as Palomar-5 are sensitive to DM substructures in the mass range 10^7–10^9 M$_\odot$. The range of median subhalo masses with V_{max} present in the right-hand panel of Fig. 3 are 1.1×10^7 to 1.6×10^8 M$_\odot$, which, while on the lower end of the quoted sensitivity range, is still within the bounds. This agreement supports our prediction that stellar streams near Magellanic-like systems may have more success that those in the vicinity of the MW-mass objects.

Indirectly, gravitational lensing searches are another avenue to probe dark matter substructure. Line ratio anomalies (Chiba 2002; Metcalf & Zhao 2002) are strongly influenced by the degree of substructure predicted in the lens system. Novel methods using adaptive optics integral field spectroscopy to measure deviations in quasar narrow line emission (Nierenberg et al. 2014) may require the expected correction due to the baryonic effects. Our results are highly relevant to such searches, suggesting LMC-mass hosts are more likely to maintain a significant amount of substructure in the mass ranges to which such methods are sensitive.

4 DWARF SATELLITES IN LMC-LIKE HOSTS

A core prediction of ΛCDM is that haloes and subhaloes act as sites of galaxy formation. We therefore expect that some fraction of the surviving dark matter subhaloes discussed above in Section 3 surrounding our LMC-mass hosts will host a luminous component consisting of stars and gas. The fact that even faint galaxies are much easier to detect than dark subhaloes makes the luminous companions of LMC-mass systems a direct and testable prediction of the galaxy formation + ΛCDM model. In light of recent results by *Gaia* regarding proper motions of several MW dwarfs, and under the assumption that the availability of 6D information allows one to reconstruct the previous associations of the LMC to other fainter dwarfs (Sales et al. 2017; Kallivayalil et al. 2018), predictions are needed on the number and distribution of visible dwarf satellites expected to orbit around Magellanic dwarfs.

Fig. 4 highlights the mapping between the stellar mass content and the maximum circular velocities of the subhaloes hosting luminous satellites with $M_* \gtrsim 1\times10^4$ M$_\odot$ of our LMC-mass hosts. At $z = 0$, the relation shows significant scatter, meaning that, at a given V_{max}, the corresponding stellar content may vary by several orders of magnitude. This effect is partially explained by the tidal stripping of subhaloes within the LMC-mass host. This is shown by the grey open symbols indicating the same relation but using the peak value ever obtained for the maximum circular velocity (V_{peak}) of each satellite, roughly corresponding to its V_{max} at infall.

Downloaded from https://academic.oup.com/mnras/article-abstract/489/4/5348/5561484 by University of Texas Libraries user on 02 October 2019

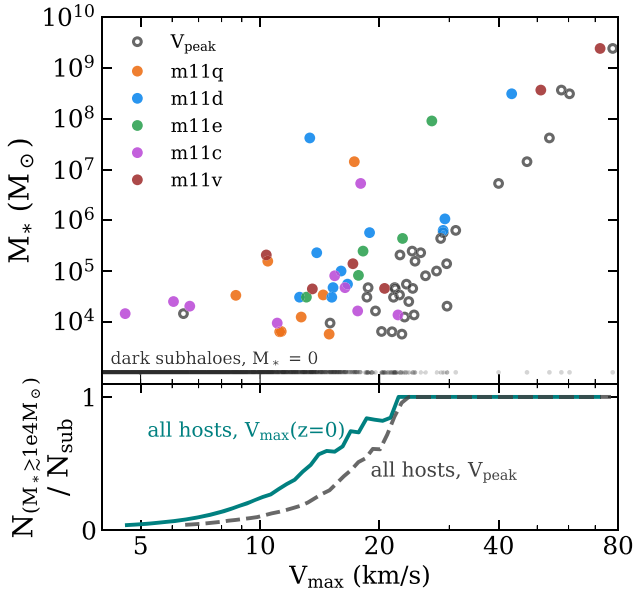

Figure 4. (Top) The $z = 0$ $V_{\rm max}$ (coloured) and the peak $V_{\rm max}$ ever obtained (grey squares) of luminous $M_* \gtrsim 1{\times}10^4$ M$_\odot$ companions within the virial radius versus their stellar mass. Subhaloes with $V_{\rm max} \lesssim 20$ km s^{-1} show a scattered relation with stellar mass, reflecting the stochastic nature of galaxy formation at this scale. (Bottom) The fraction of luminous to dark subhaloes at a given $V_{\rm max}$ or $V_{\rm peak}$, using the combined sample of all subhaloes with $d_{\rm host} < r_{\rm 200m}$ of all hosts. The galaxy occupation fraction reaches unity for subhaloes around $V_{\rm max} \sim 20$ km s^{-1}, though the distribution of current $V_{\rm max}$ has been shifted downwards, as expected due to tidal stripping of dark matter.

A similar increase in scatter in the $M_* - V_{\rm max}$ relation has been observed for satellites in MW-mass hosts (e.g. Fattahi et al. 2013), however, scatter in the $M_* - V_{\rm peak}$ relation is lower. This could have implications for abundance matching relations at small mass scales (see e.g. Garrison-Kimmel et al. 2017a). We return to tidal effects in Section 4.3. Additional factors contributing to the scatter is the stochasticity of the galaxy formation process near the low-mass end, as well as details of the assembly history of the halo and its inner dark matter density (Fitts et al. 2017).

We note that only a small fraction of the dark matter companions host a luminous dwarf companion (defined here as a galaxy within its host virial radius that has a stellar mass $M_* \gtrsim 10^4$ M$_\odot$ in `m11q`). The bottom panel of Fig. 4 shows the subhalo occupation fraction: the cumulative number of luminous $M_* \gtrsim 1{\times}10^4$ M$_\odot$ satellites at a given $V_{\rm max}$ divided by the cumulative number of dark + luminous subhaloes at that $V_{\rm max}$. We have stacked the subhaloes and companions of all hosts to achieve a more complete sample across all ranges of $V_{\rm max}$. To account for the different resolution in our runs, we only consider subhaloes above the minimum $V_{\rm max}$ thresholds introduced in Table 1 for each run.

The occupation fraction for galaxies with $M_* \gtrsim 1{\times}10^4$ M$_\odot$ quickly decreases from about unity for $V_{\rm max} \geq 20$ km s^{-1} to only a few per cent at $V_{\rm max} \sim 5$ km s^{-1}. For reference, our prediction is that about half of the subhaloes with $V_{\rm max} = 15$ km s^{-1} will host a luminous dwarf, the rest remaining dark or below the $M_* = 10^4$ M$_\odot$ resolved in our runs. These variations are commonly referred to as 'stochasticity' in the galaxy formation model, as dark matter subhaloes of comparable mass may vary their stellar content by several orders of magnitude, including remaining totally dark, and predicting the exact form of the occupation fraction as a function of $V_{\rm max}$ must consider many factors of the evolution of subhaloes, such as their merger histories and accretion time, as well as external factors such as the onset and end of reionization and the form of the ionizing background.

4.1 New proper motions from *Gaia*

From the observational side, determining the dwarf satellites associated with the LMC prior to infall into the MW is not straightforward. Since tidal stripping due to the MW potential has already begun, the material once associated with the LMC in the past does not necessarily cluster around it today. However, because the LMC is inferred to be most likely in its first pericentre passage (Kallivayalil et al. 2013), cosmological simulations suggest that the stripped material may still retain its phase-space coherence, opening an avenue to disentangle previous associations (Sales et al. 2011, 2017; Deason et al. 2015; Jethwa et al. 2016). This coherence means that all subhaloes within the LMC at infall are therefore expected to be distributed on the sky following the projection of positions and velocities of the LMC's orbit. Note that final membership requires of a combination of position on the sky, Galactocentric distance, and 3D velocity to be satisfied simultaneously.

This imposes strong constraints on the orbital poles expected for early companions of the LMC and can be used to single out possible associations. This criteria was used in Sales et al. (2011) to conclude that, with the exception of the SMC, no other classical dwarf with available proper motions at that time was consistent with an LMC association. With the arrival of new *Gaia* DR2 data, proper motions are now available for many dwarfs in the MW, including classical and UF dwarfs (we assume the cut-off for UFs to be a stellar mass of $M_* < 10^5$ M$_\odot$, as in Bullock & Boylan-Kolchin 2017). With the new 6D information, Kallivayalil et al. (2018) confirmed a likely association for four UFs: Car2, Car3, Hor1, and Hyd1. The authors suggest follow-up measurements for the confirmation of Dra2 and Hyd2, which have incomplete proper motion information. On the other hand, several of the classical dwarfs have updated proper motion measurements and their membership needs to be re-evaluated.

We have repeated the analysis in Sales et al. (2011, S11) but now using the *Gaia* DR2 proper motions presented in (Gaia Collaboration 2018, H18). In particular, for classical dwarfs satisfying the Galactocentric distance, position on the sky, and radial velocity constraints, S11 lists predictions for the orbital angular momentum expected in case of association. Following S11, we use a Cartesian coordinate system centred on the Milky Way, with x in the Sun-Galactic centre towards $l = 0°$, y towards $l = 90°$ in the direction of Galactic rotation, and z coincident with the disc angular momentum, towards $b = 90°$. For completeness, we list in Table 3 the j_x, j_y, and j_z (all normalized to $|\,\vec{j}\,|$) of all dwarfs included in H18 that were not part of the Kallivayalil et al. (2018) analysis. Errors are propagated from the quoted errors in H18 based on our calculation of j_x, j_y, and j_z. These calculated values are labelled 'obs' for each individual galaxy. However, of most relevance to this work are the dwarfs for which S11 had pre-determined possible association based on sky positions and radial velocity. For those cases, we also list the predicted angular momenta for the first pericentric passage (t_{1p}). Note that Sculptor and Leo II become a possible association only on a second-pericentric passage according to S11 (t_{2p}).

With the newest proper motions from *Gaia*, Carina, and Fornax are also compatible with having been accreted as part of the LMC system ('obs' and t_{1p} are consistent with each other within 1 σ). With stellar masses of $3.8{\times}10^5$ and $2.0{\times}10^7$ M$_\odot$, respectively, this newly confirmed pair of galaxies fills the classical dwarf scale

Downloaded from https://academic.oup.com/mnras/article-abstract/489/4/5348/5561484 by University of Texas Libraries user on 02 October 2019

Table 3. Normalized Cartesian components of satellite galaxy orbital angular momenta, as predicted by S17 for the first pericentric passage of the LMC (labelled 't_{1p}') and observed angular momenta as calculated from *Gaia* proper motions, originally tabulated in Gaia Collaboration (2018), table C.4 (labelled 'obs'). These new measurements show Carina and Fornax as being consistent with a co-infall scenario with the LMC using criteria for Magellanic Cloud system membership as defined in S17: $j_x < 0$ and $|j_x| > |j_y|, |j_z|$.

Name	Time	j_x	j_y	j_z
LMC	t_{1p}	-0.97 ± 0.03	0.14 ± 0.07	-0.19 ± 0.10
	obs	-0.93 ± 0.06	-0.1 ± 0.03	-0.36 ± 0.03
SMC	t_{1p}	-0.92 ± 0.05	0.04 ± 0.10	0.35 ± 0.08
	obs	-0.87 ± 0.06	-0.4 ± 0.04	-0.27 ± 0.04
Carina	t_{1p}	-0.93 ± 0.12	0.25 ± 0.07	-0.04 ± 0.20
	obs	$-0.97^{+0.13}_{-0.14}$	0.17 ± 0.04	-0.19 ± 0.1
Fornax	t_{1p}	-0.92 ± 0.20	0.19 ± 0.11	0.20 ± 0.07
	obs	$-0.96^{+0.23}_{-0.22}$	$-0.17^{+0.13}_{-0.14}$	0.24 ± 0.07
Sculptor	t_{2p}	-0.94 ± 0.06	-0.00 ± 0.41	0.04 ± 0.05
	obs	0.99 ± 0.01	$-0.03^{+0.08}_{-0.07}$	0.13 ± 0.01
Sagittarius	t_{1p}	–	–	–
	obs	0.05 ± 0.02	$-0.99^{+0.09}_{-0.08}$	$-0.13^{+0.08}_{-0.09}$
Ursa Minor	t_{1p}	–	–	–
	obs	-1.0 ± 0.08	-0.09 ± 0.07	-0.02 ± 0.06
Leo I	t_{1p}	–	–	–
	obs	$-0.5^{+0.4}_{-0.37}$	$-0.59^{+0.5}_{-0.48}$	$-0.64^{+0.36}_{-0.34}$
Sextans	t_{1p}	–	–	–
	obs	-0.39 ± 0.05	-0.58 ± 0.06	-0.71 ± 0.06
Leo II	t_{2p}	-0.92 ± 0.05	0.21 ± 0.21	-0.28 ± 0.15
	obs	$-0.13^{+2.26}_{-2.05}$	$0.97^{+2.24}_{-2.12}$	$0.22^{+0.88}_{-0.81}$
Bootes I	t_{1p}	–	–	–
	obs	$0.6^{+0.16}_{-0.15}$	0.71 ± 0.11	-0.31 ± 0.08
Draco	t_{1p}	–	–	–
	obs	$0.89^{+0.1}_{-0.09}$	0.36 ± 0.06	$-0.27^{+0.08}_{-0.09}$

($10^5\,M_\odot \lesssim M_* \lesssim 10^7\,M_\odot$) in the satellite mass function of the LMC, which was previously populated only by UF dwarfs (Car2, Car3, Hor1, Hyd1 aside from the from the relatively bright SMC with $M_* \sim 4.6\times10^8\,M_\odot$).

Pardy et al. (2019) suggest the possibility of LMC co-infall for Carina and Fornax by constraining their projected 2D orbital poles to within 30° of that of the LMC. We expand on this claim by using a more stringent criteria: matching angular momentum orientation with the one expected for and LMC-like debree at the same position on the sky of Carina and Fornax. Notice that the radial velocities for both dwarfs have been already found consistent with an LMC association in previous work (Sales et al. 2011, 2017). Also worth highlighting, the Galactocentric distance of Carina is in good agreement with predictions of association whereas in the case of Fornax, the measured Galactocentric distance ($\sim$ 140 kpc) places it beyond the $\sim$ 100 kpc preferred location of the debree (see for instance fig. 6 in Sales et al. 2011). The large distance of Fornax is more consistent with the scenario of a more massive infall halo mass for the LMC (whereas previous predictions were based on an LMC-analogue with $\sim$ 10 times lower mass), which would allow for a more extended distribution of the associated material. This caveat is an important one to bear in mind, and invites further investigation.

Note that Ursa Minor seems to meet the criteria set forth by S17 ($j_x < 0$ and $|j_x| >> |j_y|, |j_z|$). However, its nearly perfect radial orbit ($j_x = -1$, $j_y \approx j_z \approx 0$) as well as its position in a completely distinct region of the sky than predicted for LMC debris (and where all currently known LMC satellites reside; see S17, fig. 1) suggest a non-Magellanic origin for Ursa Minor.

We summarize in Table A1 a complete list of MW dwarfs with their current understanding of association to the LMC. The rightmost columns labelled 'possible' (if follow up is needed) and 'confirmed' (if enough information exists to make the claim) with the relevant references. The previously confirmed satellites of the LMC (by S17 and K18) include Car2, Car3, Hor1, Hyd1, and the SMC. No label means that a given galaxy is unlikely to be associated with the LMC given the current data. Galaxies confirmed by our calculations using *Gaia* DR2 are labelled 'this work'.

4.2 Simulated LMC satellite populations

With new observational context to the number of dwarf galaxies consistent with co-evolution and co-infall with the LMC, we can examine these results in a cosmological context. We provide this context by analysing the satellite population of ΛCDM cosmological zoom-in simulations of isolated LMC-mass hosts. The left-hand panel in Fig. 5 shows the stellar mass function of LMC satellites in FIRE (coloured lines refer to the same simulations as previous figures, with the dashed lines representing an extrapolation to M_* $\sim 10^4\,M_\odot$ for the runs with resolution $m_{\rm bary} = 7070\,M_\odot$). In dark grey we show the observed stellar mass function of LMC satellites inferred from the kinematics of MW dwarfs from *Gaia* DR2 data, using starred symbols for the confirmed associations (SMC, Carina, Fornax, Hyd1, Car2, Hor1, and Car3) and in triangles including all 'possible' associations to the LMC, as determined by S17 and K18.

We find an overall good agreement between the inferred satellite population of the LMC and our simulated analogues. Our simulations predict between 1 and 5 classical satellites of the LMC, in agreement with the observational estimate of 3 for the LMC (SMC, Carina, and Fornax). There is an interesting mass dependence on the ability to predict relatively massive satellites for an LMC-like host. Only the two highest mass FIRE hosts (`m11d` with $M_{200\rm m} = 2.8\times10^{11}\,M_\odot$, and `m11v` with $M_{200\rm m} = 2.9\times10^{11}\,M_\odot$) are able to reproduce the high-mass end of the LMC's satellite mass function, in very close agreement with the halo mass estimates of the LMC ($\sim3\times10^{11}\,M_\odot$) from other methods based on abundance matching (Behroozi, Wechsler & Conroy 2013b; Moster et al. 2013) and circular velocity measurements (van der Marel & Kallivayalil 2014). In fact, the average halo mass of an LMC–SMC system in the EAGLE simulations is $\sim3\times10^{11}\,M_\odot$ (Shao et al. 2018b; Cautun et al. 2019). The remaining three centrals with halo mass $\sim 1.5\times10^{11}\,M_\odot$ tend to have lower mass companions than the SMC. On the other hand, all runs have at least one satellite within a factor of two the stellar mass of Fornax, supporting its association to the LMC as suggested by the newly released *Gaia* kinematics.

One should keep in mind that the LMC–SMC association itself is rather unusual. Previous works on LMC–SMC selected pairs have showed them to be rare, though not impossible (Boylan-Kolchin et al. 2011a; Stierwalt et al. 2015). For example, Besla et al. (2018) used Illustris and SDSS to predict that the number of companions with $M_*\sim 2\times10^8\,M_\odot$ per LMC-mass dwarf is roughly 0.02 once projection effects have been taken into account. It is unclear how this figure changes with host mass, but following our results on the trend with virial mass, the likelihood of such a companion should increase if the LMC halo is on the massive end of the 1–3 $\times10^{11}\,M_\odot$ range.[6]

[6] `m11v` was specifically selected to be a multimerger, and thus cannot aid a discussion of the cosmological frequency of large satellites

Downloaded from https://academic.oup.com/mnras/article-abstract/489/4/5348/5561484 by University of Texas Libraries user on 02 October 2019

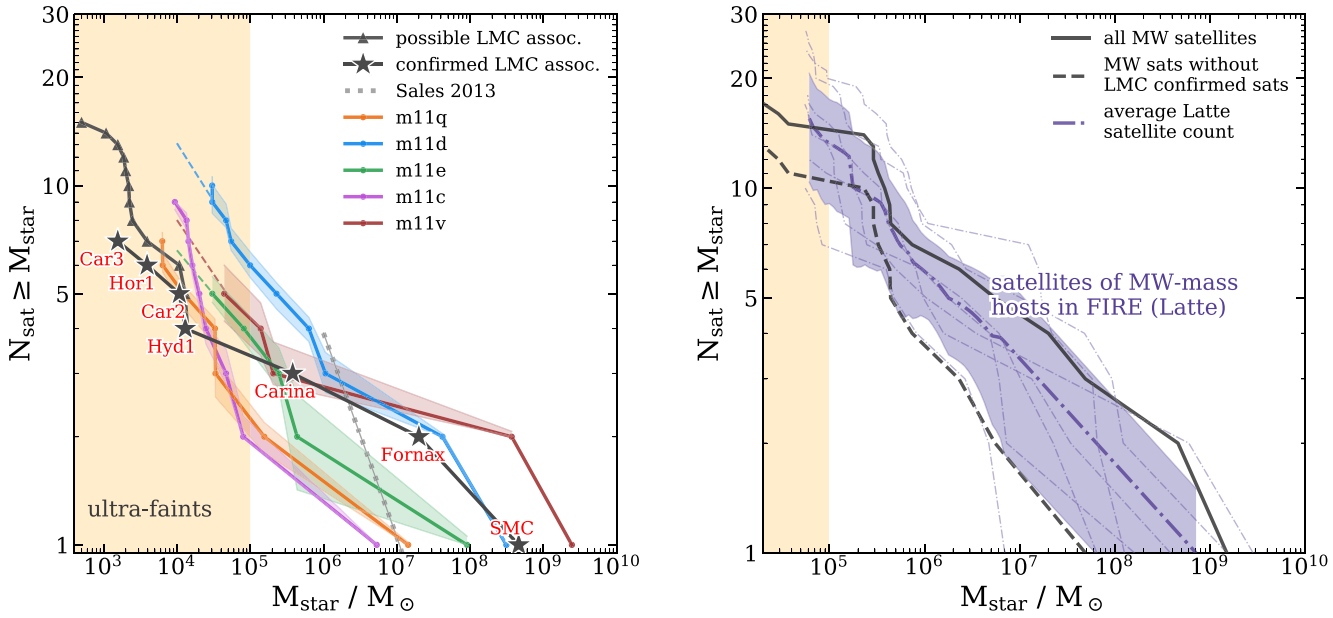

Figure 5. Cumulative $z = 0$ count of satellite galaxies above a given stellar mass within one virial radius of the host. (Left) The satellite stellar mass functions of LMC-mass hosts in FIRE (coloured) and the real LMC (dark grey). Shaded regions show the 1σ variance from over the last $\sim$1.3 Gyr. Confirmed LMC satellites are named in red and shown as star markers, while possible LMC satellites are cumulative with the confirmed population and shown as triangles. 'Confirmed LMC assoc.' refers to dwarf galaxies with full proper motion measurements which have angular momenta in agreement with the LMC infall direction, while those labelled 'possible' have incomplete proper motion data, but existing data is consistent. The teal dotted line is the expected satellite mass function of an LMC-mass host as predicted by semi-analytic modelling in Sales et al. (2013), which uses the model in Guo et al. (2011). All error bars are Poisson noise. (Right) The solid grey line represents all satellite galaxies of the MW, while the dashed grey line represents the same satellites of the MW minus the confirmed satellites of the LMC, which are shown in the left-hand panel and listed in Table 1. This shows what the *in situ* satellite population of the MW was prior to the infall of the LMC and its associated companions. The purple shaded region represents the range of satellite mass functions of these MW-mass hosts in FIRE, with thin lines representing each individual host, and thick line indicating the average number of luminous satellites at each mass. The yellow vertical shaded region on the left represents the UF mass scale.

In general, the number of classical dwarfs in our FIRE centrals is in good agreement with earlier predictions from semi-analytical calculations in Sales et al. (2013, light-blue dotted line) taken from the Millennium-II simulations (Boylan-Kolchin et al. 2009). However, the overall slope on the massive end of the FIRE runs is shallower than that in Sales et al. (2013), probably a result of a slightly different stellar mass–halo mass relation for low-mass dwarfs in the semi-analytical catalogue than in our hydrodynamical runs.

For the UF regime, our two highest resolution runs, `m11q` and `m11c`, predict 5–8 companions with $M_* \geq 10^4$ M$_\odot$, which is in good agreement with the 5 inferred for the LMC from proper motion observations of MW dwarfs (Kallivayalil et al. 2018). In general, if extrapolating the medium-resolution runs to $M_* \geq 10^4$ M$_\odot$ (which, according to the highest resolution runs, would be a reasonable approach) the predicted number of satellites above this stellar mass may be as high as 11 for `m11d`. Although such predictions should be taken with caution given the low number statistics and numerical resolution, the assumption that some of the LMC UF companions still await discovery is a reasonable one. In particular some of the brighter 'possible' associations already identified, Hyd2 with $M_* \sim 1.4\times10^4$ M$_\odot$ and Dra2 with $M_* \sim 2.5\times10^3$ M$_\odot$, might deserve a closer follow up to confirm or rule out their Magellanic origin.

Furthermore, our estimates for the number of ultra-faint companions can be regarded as lower limits, because of the implemented model for cosmic ray heating in the ISM (in addition to the assumed UV background), which in these FIRE simulations induces too much heating in gas at early times ($z \gtrsim 10$) (Garrison-Kimmel et al. 2019). This effect has been explicitly tested with no observed impact on the population of classical dwarfs, however, the additional heating may in fact *decrease* the number of predicted UFs compared to a method resulting in later reionization (for details, see Garrison-Kimmel et al. 2019, section 3.3 and appendix B). As such, our estimates are effectively a conservative lower limit and indicate that several yet-to-be-discovered companions to the LMC may yet exist.

Lastly, on the right-hand panel of Fig. 5 we show the observed stellar mass function of MW satellites (black solid) along with satellites of M31 (black dot dashed). If the LMC brought along several of the dwarfs as estimated from the previous calculations (grey starred symbols), the MW satellite mass function must have looked rather different about 1 Gyr ago right before the infall of the LMC.[7] This is shown as the grey dashed line, computed as the total MW satellites but subtracting the confirmed LMC associations. As usual, we define satellites as those within r_{200m} of the host. In such case, the MW halo may have hosted a significantly lower number of dwarfs than now, although still in reasonable agreement with the predicted satellite population of Latte galaxies ($M_{200m} \sim 10^{12}$ M$_\odot$, shaded in purple). The similarity between the high-mass end of the satellite mass function for the MW and the LMC argues once again for a rather massive pre-infall LMC halo, likely $\sim 3 \times 10^{11}$ M$_\odot$ and above, predicting several undiscovered UF dwarfs that were previously associated with the LMC.

[7]However, exact counts of luminous satellites are subject to change over this time-scale as they are disrupted into streams, e.g. Sagittarius.

Downloaded from https://academic.oup.com/mnras/article-abstract/489/4/5348/5561484 by University of Texas Libraries user on 02 October 2019

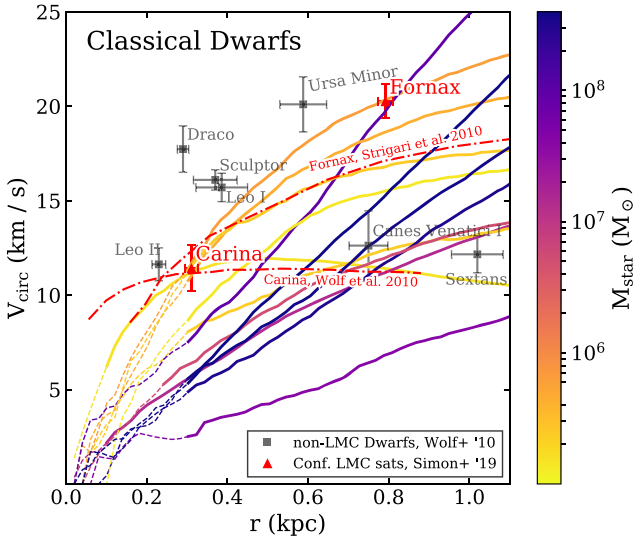

Figure 6. Circular velocity profiles $\left(V_{\rm circ} = \sqrt{GM(<r)/r}\right)$ of all `m11` satellites in FIRE. Due to resolution, only satellites with M_* above (below) 1×10^5 M$_\odot$ are shown, coloured according to M_*. All individual points are observed half-light radii (*x-axis)* versus $V_{\rm circ}(r_{1/2}) = \sqrt{3\langle\sigma^2_{\rm los}\rangle}$ as described in Boylan-Kolchin, Bullock & Kaplinghat (2012). Grey points (taken from Wolf et al. 2010) are various MW dwarfs that do not belong to the LMC system, while those dwarf galaxies presumably associated with the LMC are painted in red. The two red lines are circular velocities for Carina and Fornax as determined by Strigari, Frenk & White (2010) and Wolf et al. (2010), noted accordingly. The dark matter content of our predicted classical satellites is in good agreement with the newly deemed members, Carina and Fornax.

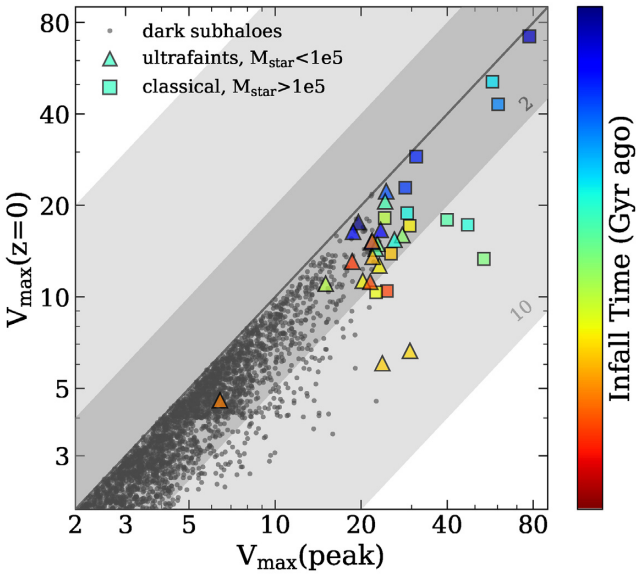

Figure 7. The peak $V_{\rm max}$ ever obtained by the subhalo versus its present-day $V_{\rm max}$. Squares represent subhaloes which host galaxies of $M_*\geq 10^5$ M$_\odot$, triangles host those with $M_*\leq 10^5$ M$_\odot$, and grey dots are dark subhaloes. The colour bar shows the time in Gyr since a given satellite's infall to the host LMC-mass central. As expected, satellites with recent infall times ($T_{\rm inf}\lesssim 4$ Gyr) show minimal deviation from $V_{\rm peak}$. However, tidal disruption within LMC-mass systems for earlier infalling satellites may cause a factor of $\sim$ 2–7 reduction in the $V_{\rm max}$ of UFs at $z = 0$.

4.3 The predicted dark matter content of LMC satellites

Besides the number of dwarf galaxies expected around Magellanic-like systems, a further (arguably stronger) test for ΛCDM galaxy formation models is to reproduce the internal kinematics of the stars that are measured from observations. In the case of UF dwarfs, reported velocities from observations cover mostly the radius range $r < 200$ pc; with at least half of the systems having measured velocities within 50 pc (Simon 2019). Unfortunately, integrated quantities such as circular velocities are not yet converged in our simulations at such extreme small radii (typical gravitational softening $\epsilon_{\rm DM} \sim$ 20–40 pc for all runs). We therefore analyse kinematic profiles of simulated classical dwarfs, but present a study of $V_{\rm max}$ that can guide the conclusions in the UF regime.

Fig. 6 shows the circular velocity profiles of all simulated classical satellites ($M_* > 10^5$ M$_\odot$) of our FIRE LMC-analogues. Lines are dashed below the dark matter convergence radius for each resolution as listed in Hopkins et al. (2018b). Individual curves are colour coded according to the stellar mass content of each satellite, as indicated by the colour bar. The simulation data hints to a correlation where the larger M_* dwarfs will populate larger circular velocity subhaloes, at least in the regime of classical dwarfs.

Observed dwarf spheroidals are also plotted as single points assuming $V_{\rm circ}(r_{1/2}) = \sqrt{3\langle\sigma_{\rm los}\rangle}$ with $\sigma_{\rm los}$ the observed line-of-sight stellar velocity on the y-axis and the half-light radii $r_{1/2}$ on the x-axis (following Boylan-Kolchin et al. 2012). Sources for the observed $\sigma_{v,*}$ are listed in the legend of Fig. 6. Observed galaxies presumably associated with the LMC are shown in red while other MW dwarfs are plotted in grey. For completeness, we also include the full circular velocity profiles as a function of radius for Carina and Fornax from Wolf et al. (2010) and Strigari et al. (2010), respectively.

The predicted mass content for the brightest satellites of LMC-mass hosts, such as Carina and Fornax, are consistent with the observational values, supporting the possible association to the LMC inferred from their proper motions. It is important to highlight that the simulated curves in Fig. 6 are, if anything, lower limits to the true density of simulated dwarfs, as a smaller softening and increased resolution would result in higher inner velocities,[8] which would still accommodate the observed values. The good agreement with observations of Carina and Fornax is therefore encouraging and highly suggestive of a possible membership to the LMC group.

For the UF regime, we turn our analysis to maximum circular velocities, as we expect them to be well converged. Following equation 10 in Springel et al. (2008), the correction due to numerical effects is at most $\sim$0.1 km s^{-1}, or $\lesssim$1 per cent. Interestingly, a closer inspection of our simulations reveals that tidal stripping is likely to play a major role on the present-day dark matter content of LMC companions, particularly in the UF regime. This is clearly seen in Fig. 7, which shows a comparison between peak maximum circular velocity achieved throughout a subhalo's history ($V_{\rm peak}$) as a function of the circular velocity measured at present day [$V_{\rm max}(z = 0)$] for all subhaloes in our sample of LMC-mass hosts in FIRE. Dark subhaloes are indicated with grey dots, while large squares and triangles highlight the location of classical and UF simulated dwarfs, respectively. The symbols are colour coded by lookback time since accretion (lower values are more recent infalls), and confirm that some of the surviving UF satellites in an LMC system may have been accreted as early as 12 Gyr ago. The two

[8]We have tested this explicitly, see Fig. A2. Also see Springel et al. (2008) for an evaluation of softening effects on $V_{\rm circ}$.

Downloaded from https://academic.oup.com/mnras/article-abstract/489/4/5348/5561484 by University of Texas Libraries user on 02 October 2019

regions of dark and light shaded grey indicate factors of 2 and 10 decrease in circular velocity.

As indicated by Fig. 7, the UF LMC companions are narrowly distributed at $V_{\rm peak} \sim 20$ km s^{-1} at infall but show a large spread in $V_{\rm circ}$ today, 6–20 km s^{-1}. We find the present-day median $V_{\rm max}$ for UF LMCs to be 14.4 km s^{-1}. As expected, the latest ones to infall remain close to the 1-to-1 line, as tidal disruption has not had sufficient time to affect their properties. We find that he amount of tidal stripping experienced is not dependent on stellar mass. However, consider (*i*) the narrow range of $V_{\rm peak}$ predicted for UFs, and (*ii*) their low stellar masses, at which feedback is not expected to affect the inner DM distribution. Both effects combined establish an interesting correlation in UFs that might be used to assess their likelihood of association to the LMC. We emphasize that low central densities are a necessary rather than sufficient condition to determine an association to the LMC since an early infall on to the MW for UFs will also induce tidal stripping and associated lower inner densities. Determining which host a satellite was first associated with is a task left to orbital phase-space analysis, as in Section 4.1.

Although tidal stripping proceeds mostly outside-in, subhaloes that are affected by tides also register a drop in their inner dark matter content (e.g. Hayashi et al. 2003; Brooks & Zolotov 2014). It is therefore expected that UF satellites of the LMC might show lower inner velocities than objects of similar mass that were accreted more recently into the MW. This prospect is interesting since *Gaia* DR2 data suggest that several of the UF galaxies are likely on their first infall on to the MW (Simon 2018). Identifying UF dwarfs with orbital properties consistent with that of the LMC and that simultaneously show the lowest inner densities may help to constrain the most likely LMC group members.[9] From that perspective, the likely associations for Hyd1 with $V_{\rm circ} = 4.7$ km s^{-1} and Car2 with $V_{\rm circ} = 5.9$ km s^{-1}, both within $r \leq 100$ pc, or the possibly associated Hyd2 with $V_{\rm circ} = 6.2$ km s^{-1}, seem favoured compared to the more dense Car3, Hor1, or Dra2 with $V_{\rm circ} \geq 8$ km s^{-1} at $r \sim 50$ pc (data from Simon 2019). However, higher resolution simulations as well as more accurate observations are needed in order to make more definitive claims.

5 SUMMARY AND CONCLUSIONS

We used five ΛCDM cosmological zoom in simulations of LMC-mass hosts ($M_{\rm 200m} = 1$–3×10^{11} M$_\odot$) in FIRE to examine both the dark and luminous substructure of such galaxies, against which we compare to the Latte suite of seven simulations of MW-mass hosts. We summarize our primary findings here, and discuss our conclusions in the following paragraphs.

(i) By comparing DMO to hydrodynamic baryonic simulations, we show that suppression of dark matter substructure is less strong for LMC-mass hosts than for MW-mass hosts, since this suppression is caused by tidal interactions with the central baryonic galaxy (Garrison-Kimmel et al. 2017b). We therefore expect that LMC-mass galaxies are promising laboratories for subhalo detection.

(ii) We calculate orbital angular momenta for 10 observed MW-dwarfs using *Gaia* DR2 data (Gaia Collaboration 2018) and show that Fornax and Carina are highly consistent with predictions for tidal debris of a simulated LMC-MW infall scenario from Sales et al. (2017). This brings the inferred satellite mass function of the LMC up to seven members, including the SMC and the four UFs identified in Kallivayalil et al. (2018).

(iii) We compare this to the simulated satellite mass function of our five LMC-mass hosts in FIRE and find excellent agreement on the bright end with our higher mass haloes. Our simulations suggest that more UFs are expected for a halo comparable to that of the LMC. In addition, the population of MW satellites pre-LMC infall remains consistent with simulated MW-mass hosts in FIRE.

(iv) We find that the tidal disruption of simulated LMC satellites, indicated by a reduction in their maximum circular velocities after infall, is an important effect, even at such host mass scales. We therefore expect that dwarfs associated with the LMC should have lowered densities, though this is not sufficient criteria for association by itself as tidal effects from the MW are also expected to affect nearby dwarfs.

We have shown that LMC-mass centrals suppress much less dark matter substructure compared to MW-mass centrals, with a particularly striking difference in suppression patterns for the inner 0.2 $r_{\rm 200m}$ of the halo. There, we observe a factor of ∼3.5 reduction (from DMO to baryonic runs) in the number of subhaloes at $V_{\rm max} = 10$ km s^{-1} in MW mass hosts versus a factor of ∼1.4 for LMC mass hosts. This suppression of substructure is mainly due to tidal interactions with the central baryonic disc. We identify two features of the LMC-mass hosts in FIRE that explains this: (i) a much lower stellar mass to halo mass ratio than that of MW-mass objects and (ii) a significantly shallower inner density profile (larger core). The first implies that the gravitational potential of the galaxy is less significant compared to that of the halo. The second implies that the shape of the potential is much smoother than that seen in DMO versions of similar haloes and that seen in haloes hosting larger central galaxies. This combination provides a friendlier environment in the baryonic runs of cored $M_{\rm 200m} \sim 10^{11}$ M$_\odot$ haloes, leading to less suppression of subhaloes due to tidal disruption on these scales compared to the harsher effects reported for 10^{12} M$_\odot$ hosts (D'Onghia et al. 2010; Garrison-Kimmel et al. 2017b; Samuel et al. 2019).

We compare the simulated satellite population of the LMC-mass hosts to the set of observed MW dwarfs that is consistent with an LMC co-infall scenario. We present revised calculations following Sales et al. (2011) and using updated *Gaia* DR2 proper motion for classical dwarfs ($M_* \geq 10^5$ M$_\odot$) from Gaia Collaboration (2018). We find that Carina and Fornax are now compatible with a common infall along with the LMC system, and are added to the previously suggested associations to the SMC and the group of UF candidates Car2, Car3, Hor1, and Hyd1 introduced in Kallivayalil et al. (2018). We find generally good agreement with the satellite population inferred for the real LMC. One of our haloes, `m11d` with $M_{\rm 200m} \sim 3 \times 10^{11}$ M$_\odot$, is able to accurately predict the mass distribution of the three largest LMC satellites: the SMC, Fornax, and Carina, providing theoretical support to the claims of association. Furthermore, the predicted circular velocities for LMC satellites in this mass range are in good agreement with measurements of Carina and Fornax.

For fainter satellites, the LMC-mass systems in FIRE host comparable to slightly more UF companions than observed with the real LMC. On average, 7 ± 2 satellites are predicted above $M_* = 10^4$ M$_\odot$, in reasonable agreement with the 5 above that mass limit presumed associated with the LMC (Car2, Hyd1, Carina, Fornax, and the SMC). We find that UF companions of the LMC are expected to have experienced significant tidal disruption within the LMC

[9]Note that the MW environment may also be conducive to tidal stripping such that low inner densities may be a telling but not sufficient condition for association to the LMC.

Downloaded from https://academic.oup.com/mnras/article-abstract/489/4/5348/5561484 by University of Texas Libraries user on 02 October 2019

potential, as measured by the decrease on the subhalo maximum circular velocities since infall. As such, lower dark matter inner densities together with their orbital parameters (Kallivayalil et al. 2018), may help identify those ultrafaint dwarfs that infalled on to the MW as part of the LMC group.

In summary, if the SMC, Carina, and Fornax are former satellites of the LMC, this may favour a relatively massive dark matter halo mass for the LMC prior to infall on to the MW, $M_{200m} \sim 3 \times 10^{11}$ $M_\odot$. This would push the expected UF dwarf numbers to the upper end of our predicted range, suggesting that some LMC associations still await discovery. According to our simulations, the missing dwarfs will lie roughly 30–80 kpc from the LMC at infall and have $M_* \sim 10^4$ $M_\odot$ and $V_{max} \approx 15$ km s^{-1}. This implies a relatively low central dark matter density that can be used as an additional membership criteria to discern from other, more recent individual infalls on to the MW. Based on their partially known orbital parameters and their low-velocity estimates, the most promising candidate is Hyd2. Follow-up observations are needed to confirm or dismiss the association.

In addition to LMC, this work presents the first observational and testable predictions using hydrodynamical cosmological simulations for the satellite mass function of a Magellanic–mass system down to the UF regime (semi-analytic modelling has been used for similar predictions, e.g. Dooley et al. 2017; Bose, Deason & Frenk 2018). Similar to how the study of satellite population of MW-mass hosts pushed forward our understanding of galaxy formation and cosmology in the past, the large predicted number of isolated dwarfs combined with upcoming deep surveys and wide field-of-view instruments such as WFIRST, as well as searches for satellites of LMC-mass hosts beyond the MW (e.g. MADCASH; Carlin et al. 2016), may turn the study of dwarf–dwarf systems into a valuable and essential test of the ΛCDM model.

ACKNOWLEDGEMENTS

The authors would like to thank Phil Hopkins for facilitating access to the FIRE runs and stimulating discussions of the simulations and science herein. We also thank Coral Wheeler, Shea Garrison-Kimmel, and the rest of the FIRE Local Universe collaboration for their thought-provoking insight and advice. We are grateful to the anonymous referee for a constructive report that helped improve this manuscript, as well as to Marius Cautun and Marcel Pawlowski for their helpful suggestions. LVS acknowledges support from NASA through the *HST* Programs AR-14582, AR-14583 and from the Hellman Foundation. AW was supported by NASA, through ATP grant 80NSSC18K1097 and *HST* grants GO-14734 and AR-15057 from STScI. MBK acknowledges support from NSF grant AST-1517226 and CAREER grant AST-1752913 and from NASA grants NNX17AG29G and *HST*-AR-14282, *HST*-AR-14554, *HST*-AR-15006, and *HST*-GO-14191 from the Space Telescope Science Institute, which is operated by AURA, Inc., under NASA contract NAS5-26555. TKC was supported by NSF grant AST-1715101 and the Cottrell Scholar Award from the Research Corporation for Science Advancement. We ran simulations using XSEDE supported by NSF grant ACI-1548562, Blue Waters via allocation PRAC NSF.1713353 supported by the NSF, and NASA HEC Program through the NAS Division at Ames Research Center.

REFERENCES

Abadi M. G., Navarro J. F., Steinmetz M., Eke V. R., 2003, ApJ, 591, 499
Bechtol K. et al., 2015, ApJ, 807, 50
Behroozi P. S., Conroy C., Wechsler R. H., 2010, ApJ, 717, 379
Behroozi P. S., Wechsler R. H., Wu H.-Y., 2013a, ApJ, 762, 109
Behroozi P. S., Wechsler R. H., Conroy C., 2013b, ApJ, 770, 57
Besla G. et al., 2018, MNRAS, 480, 3376
Bose S., Deason A. J., Frenk C. S., 2018, ApJ, 863, 123
Boylan-Kolchin M., Springel V., White S. D. M., Jenkins A., Lemson G., 2009, MNRAS, 398, 1150
Boylan-Kolchin M., Besla G., Hernquist L., 2011a, MNRAS, 414, 1560
Boylan-Kolchin M., Bullock J. S., Kaplinghat M., 2011b, MNRAS, 415, L40
Boylan-Kolchin M., Bullock J. S., Kaplinghat M., 2012, MNRAS, 422, 1203
Brooks A. M., Zolotov A., 2014, ApJ, 786, 87
Brooks A. M., Kuhlen M., Zolotov A., Hooper D., 2013, ApJ, 765, 22
Bryan G. L., Norman M. L., 1998, ApJ, 495, 80
Bullock J. S., Boylan-Kolchin M., 2017, ARA&A, 55, 343
Bullock J. S., Kravtsov A. V., Weinberg D. H., 2000, ApJ, 539, 517
Carlberg R. G., Grillmair C. J., Hetherington N., 2012, ApJ, 760, 75
Carlin J. L. et al., 2016, ApJ, 828, L5
Cautun M., Deason A. J., Frenk C. S., McAlpine S., 2019, MNRAS, 483, 2185
Chan T. K., Kereš D., Oñorbe J., Hopkins P. F., Muratov A. L., Faucher-Giguère C. A., Quataert E., 2015, MNRAS, 454, 2981
Chan T. K., Kereš D., Wetzel A., Hopkins P. F., Faucher-Giguère C. A., El-Badry K., Garrison-Kimmel S., Boylan-Kolchin M., 2018, MNRAS, 478, 906
Chiba M., 2002, ApJ, 565, 17
D'Onghia E., Lake G., 2008, ApJ, 686, L61
D'Onghia E., Springel V., Hernquist L., Keres D., 2010, ApJ, 709, 1138
Deason A. J., Wetzel A. R., Garrison-Kimmel S., Belokurov V., 2015, MNRAS, 453, 3568
Di Cintio A., Brook C. B., Dutton A. A., Macciò A. V., Stinson G. S., Knebe A., 2014, MNRAS, 441, 2986
Dooley G. A., Peter A. H. G., Carlin J. L., Frebel A., Bechtol K., Willman B., 2017, MNRAS, 472, 1060
Drlica-Wagner A. et al., 2015, ApJ, 813, 109
El-Badry K., Wetzel A., Geha M., Hopkins P. F., Kereš D., Chan T. K., Faucher-Giguère C.-A., 2016, ApJ, 820, 131
El-Badry K., Wetzel A. R., Geha M., Quataert E., Hopkins P. F., Kereš D., Chan T. K., Faucher-Giguère C.-A., 2017, ApJ, 835, 193
El-Badry K. et al., 2018a, MNRAS, 473, 1930
El-Badry K. et al., 2018b, MNRAS, 477, 1536
Escala I. et al., 2018, MNRAS, 474, 2194
Fattahi A., Navarro J. F., Starkenburg E., Barber C. R., McConnachie A. W., 2013, MNRAS, 431, L73
Faucher-Giguère C.-A., Lidz A., Zaldarriaga M., Hernquist L., 2009, ApJ, 703, 1416
Ferrero I., Abadi M. G., Navarro J. F., Sales L. V., Gurovich S., 2012, MNRAS, 425, 2817
Fitts A. et al., 2017, MNRAS, 471, 3547
Gaia Collaboration, 2018, A&A, 616, A12
Gao L., White S. D. M., Jenkins A., Stoehr F., Springel V., 2004, MNRAS, 355, 819
Garrison-Kimmel S., Boylan-Kolchin M., Bullock J. S., Lee K., 2014, MNRAS, 438, 2578
Garrison-Kimmel S., Bullock J. S., Boylan-Kolchin M., Bardwell E., 2017a, MNRAS, 464, 3108
Garrison-Kimmel S. et al., 2017b, MNRAS, 471, 1709
Garrison-Kimmel S. et al., 2018, MNRAS, 481, 4133
Garrison-Kimmel S. et al., 2019, MNRAS, 1262
Giocoli C., Tormen G., van den Bosch F. C., 2008, MNRAS, 386, 2135
Governato F. et al., 2004, ApJ, 607, 688
Graus A. S., Bullock J. S., Kelley T., Boylan-Kolchin M., Garrison-Kimmel S., Qi Y., 2019, MNRAS, 488, 4585
Griffen B. F., Ji A. P., Dooley G. A., Gómez F. A., Vogelsberger M., O'Shea B. W., Frebel A., 2016, ApJ, 818, 10
Guo Q., White S., Li C., Boylan-Kolchin M., 2010, MNRAS, 404, 1111
Guo Q. et al., 2011, MNRAS, 413, 101
Hahn O., Abel T., 2011, MNRAS, 415, 2101

Downloaded from https://academic.oup.com/mnras/article-abstract/489/4/5348/5561484 by University of Texas Libraries user on 02 October 2019

Hayashi E., Navarro J. F., Taylor J. E., Stadel J., Quinn T., 2003, ApJ, 584, 541
Hopkins P. F., 2015, MNRAS, 450, 53
Hopkins P. F., Narayanan D., Murray N., 2013, MNRAS, 432, 2647
Hopkins P. F. et al., 2018a, MNRAS, 477, 1578
Hopkins P. F. et al., 2018b, MNRAS, 480, 800
Jenkins A. et al., 1998, ApJ, 499, 20
Jethwa P., Erkal D., Belokurov V., 2016, MNRAS, 461, 2212
Kallivayalil N., van der Marel R. P., Besla G., Anderson J., Alcock C., 2013, ApJ, 764, 161
Kallivayalil N. et al., 2018, ApJ, 867, 19
Katz N., White S. D. M., 1993, ApJ, 412, 455
Kelley T., Bullock J. S., Garrison-Kimmel S., Boylan-Kolchin M., Pawlowski M. S., Graus A. S., 2019, MNRAS, 487, 4409
Kim D., Jerjen H., 2015, ApJ, 808, L39
Kirby E. N., Bullock J. S., Boylan-Kolchin M., Kaplinghat M., Cohen J. G., 2014, MNRAS, 439, 1015
Klypin A., Kravtsov A. V., Valenzuela O., Prada F., 1999, ApJ, 522, 82
Koposov S. E., Rix H.-W., Hogg D. W., 2010, ApJ, 712, 260
Koposov S. E., Belokurov V., Torrealba G., Evans N. W., 2015, ApJ, 805, 130
Koposov S. E. et al., 2018, MNRAS, 479, 5343
Kravtsov A. V., Berlind A. A., Wechsler R. H., Klypin A. A., Gottlöber S., Allgood B. O., Primack J. R., 2004, ApJ, 609, 35
Kroupa P., 2001, MNRAS, 322, 231
Krumholz M. R., Gnedin N. Y., 2011, ApJ, 729, 36
Laevens B. P. M. et al., 2015, ApJ, 813, 44
Leitherer C. et al., 1999, ApJS, 123, 3
Lynden-Bell D., Lynden-Bell R. M., 1995, MNRAS, 275, 429
Ma X., Hopkins P. F., Faucher-Giguère C.-A., Zolman N., Muratov A. L., Kereš D., Quataert E., 2016, MNRAS, 456, 2140
McConnachie A. W., 2012, AJ, 144, 4
Metcalf R. B., Zhao H., 2002, ApJ, 567, L5
Moore B., Ghigna S., Governato F., Lake G., Quinn T., Stadel J., Tozzi P., 1999, ApJ, 524, L19
Moster B. P., Naab T., White S. D. M., 2013, MNRAS, 428, 3121
Navarro J. F., Frenk C. S., White S. D. M., 1996, ApJ, 462, 563
Nierenberg A. M., Treu T., Wright S. A., Fassnacht C. D., Auger M. W., 2014, MNRAS, 442, 2434
Okamoto T., Frenk C. S., 2009, MNRAS, 399, L174
Oñorbe J., Boylan-Kolchin M., Bullock J. S., Hopkins P. F., Kereš D., Faucher-Giguère C.-A., Quataert E., Murray N., 2015, MNRAS, 454, 2092
Orr M. E. et al., 2018, MNRAS, 478, 3653
Pardy S. A. et al., 2019, preprint (arXiv:1904.01028)
Peñarrubia J., Benson A. J., Walker M. G., Gilmore G., McConnachie A. W., Mayer L., 2010, MNRAS, 406, 1290
Pontzen A., Governato F., 2012, MNRAS, 421, 3464
Power C., Navarro J. F., Jenkins A., Frenk C. S., White S. D. M., Springel V., Stadel J., Quinn T., 2003, MNRAS, 338, 14
Press W. H., Schechter P., 1974, ApJ, 187, 425
Price D. J., Monaghan J. J., 2007, MNRAS, 374, 1347
Read J. I., Wilkinson M. I., Evans N. W., Gilmore G., Kleyna J. T., 2006, MNRAS, 367, 387
Sales L. V., Navarro J. F., Abadi M. G., Steinmetz M., 2007, MNRAS, 379, 1464
Sales L. V., Navarro J. F., Cooper A. P., White S. D. M., Frenk C. S., Helmi A., 2011, MNRAS, 418, 648
Sales L. V., Wang W., White S. D. M., Navarro J. F., 2013, MNRAS, 428, 573
Sales L. V., Navarro J. F., Kallivayalil N., Frenk C. S., 2017, MNRAS, 465, 1879
Samuel J. et al., 2019, preprint (arXiv:1904.11508)
Sawala T. et al., 2016, MNRAS, 457, 1931
Sawala T., Pihajoki P., Johansson P. H., Frenk C. S., Navarro J. F., Oman K. A., White S. D. M., 2017, MNRAS, 467, 4383
Shao S., Cautun M., Frenk C. S., Grand R. J. J., Gómez F. A., Marinacci F., Simpson C. M., 2018a, MNRAS, 476, 1796
Shao S., Cautun M., Deason A. J., Frenk C. S., Theuns T., 2018b, MNRAS, 479, 284
Simon J. D., 2018, ApJ, 863, 89
Simon J. D., 2019, Annual Review of Astronomy and Astrophysics, 57, 375
Simpson C. M., Grand R. J. J., Gómez F. A., Marinacci F., Pakmor R., Springel V., Campbell D. J. R., Frenk C. S., 2018, MNRAS, 478, 548
Somerville R. S., 2002, ApJ, 572, L23
Springel V., 2005, MNRAS, 364, 1105
Springel V. et al., 2005, Nature, 435, 629
Springel V. et al., 2008, MNRAS, 391, 1685
Stierwalt S., Besla G., Patton D., Johnson K., Kallivayalil N., Putman M., Privon G., Ross G., 2015, ApJ, 805, 2
Strigari L. E., Frenk C. S., White S. D. M., 2010, MNRAS, 408, 2364
Su K.-Y., Hopkins P. F., Hayward C. C., Faucher-Giguère C.-A., Kereš D., Ma X., Robles V. H., 2017, MNRAS, 471, 144
Tegmark M., Silk J., Rees M. J., Blanchard A., Abel T., Palla F., 1997, ApJ, 474, 1
Tollerud E. J., Boylan-Kolchin M., Bullock J. S., 2014, MNRAS, 440, 3511
Tollet E. et al., 2016, MNRAS, 456, 3542
Torrealba G. et al., 2016, MNRAS, 463, 712
Torrealba G. et al., 2018, MNRAS, 475, 5085
van der Marel R. P., Kallivayalil N., 2014, ApJ, 781, 121
Wang L., Dutton A. A., Stinson G. S., Macciò A. V., Penzo C., Kang X., Keller B. W., Wadsley J., 2015, MNRAS, 454, 83
Wetzel A. R., Nagai D., 2015, ApJ, 808, 40
Wetzel A. R., Deason A. J., Garrison-Kimmel S., 2015, ApJ, 807, 49
Wetzel A. R., Hopkins P. F., Kim J.-h., Faucher-Giguère C.-A., Kereš D., Quataert E., 2016, ApJ, 827, L23
Wheeler C., Oñorbe J., Bullock J. S., Boylan-Kolchin M., Elbert O. D., Garrison-Kimmel S., Hopkins P. F., Kereš D., 2015, MNRAS, 453, 1305
Wheeler C. et al., 2018, preprint (arXiv:1812.02749)
White S. D. M., Rees M. J., 1978, MNRAS, 183, 341
Wolf J., Martinez G. D., Bullock J. S., Kaplinghat M., Geha M., Muñoz R. R., Simon J. D., Avedo F. F., 2010, MNRAS, 406, 1220
Wright A. H. et al., 2017, MNRAS, 470, 283
Yang X., Mo H. J., van den Bosch F. C., 2003, MNRAS, 339, 1057
Yang X., Mo H. J., Zhang Y., van den Bosch F. C., 2011, ApJ, 741, 13
Yoon J. H., Johnston K. V., Hogg D. W., 2011, ApJ, 731, 58

APPENDIX A: ADDITIONAL INFORMATION

Here we include additional information relevant to the discussions above. We test the effects of resolution in our simulations by comparing the subhaloes of `m11q` run at the 'high' and 'normal' resolutions as described in Section 2.2. We examine the subhalo $V_{\rm max}$ functions as described in Section 2.1 in Fig. A1 and the circular velocity profiles of subhaloes with 8 km s^{-1} $< V_{\rm max} <$ 12 km s^{-1} as described in Section 4.3 in Fig. A2. We examine the radial distribution of subhaloes in LMC-mass hosts and MW-mass hosts as described in Section 3.1 in Fig. A3. We include our observational data set as described in Section 4.1 in Table A1, including stellar mass, Galactocentric coordinates and radial velocities, distance to the LMC, as well as the current status of association to the LMC system.

Downloaded from https://academic.oup.com/mnras/article-abstract/489/4/5348/5561484 by University of Texas Libraries user on 02 October 2019

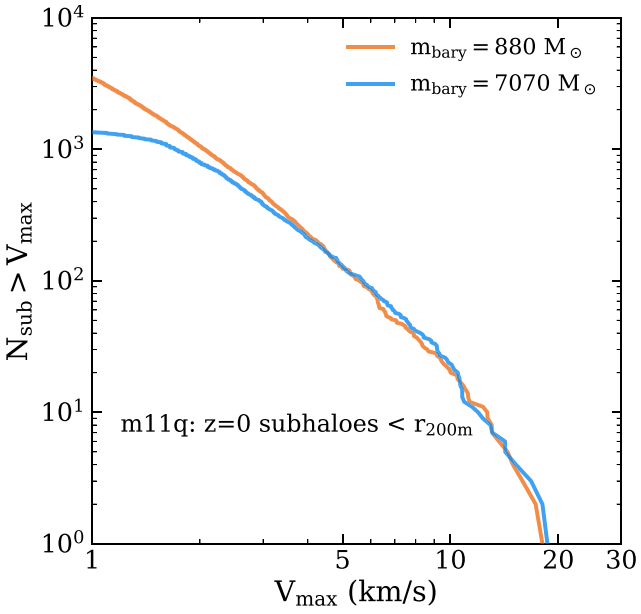

Figure A1. Resolution convergence of the $z = 0$ subhalo population of `m11q` at two resolutions: $m_{\rm bary} = 7070\ {\rm M}_\odot$ (blue) and $m_{\rm bary} = 880\ {\rm M}_\odot$ (orange). The populations diverge below the typical value ($\sim$4 km s^{-1}) used for our minimum subhalo $V_{\rm max}$ cut-off in Section 3, meaning the subhalo populations used in that analysis are well converged.

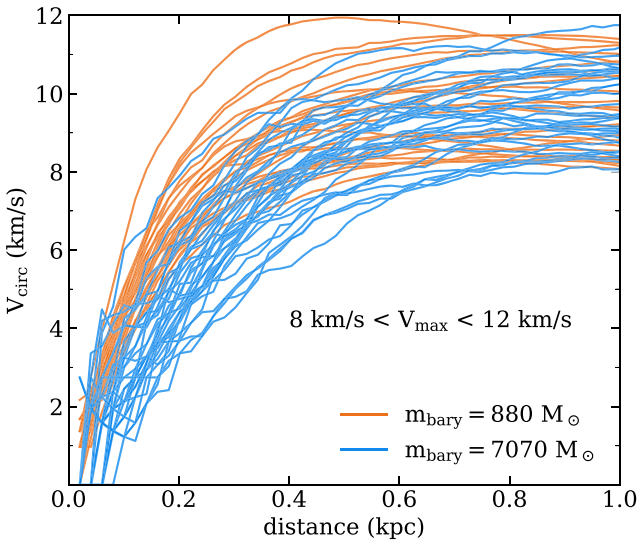

Figure A2. Circular velocity profiles ($V_{\rm circ} = \sqrt{GM(<r)/r}$) of subhaloes with 8 km s^{-1} < $V_{\rm max}$ < 12 km s^{-1} in `m11q` in high resolution ($m_{\rm bary}$ = 880 M$_\odot$, orange) and the lowest resolution included herein ($m_{\rm bary}$ = 7070 M$_\odot$, blue). The lower resolution run shows a systematic underdensity until convergence is reached at $r \sim 0.8$ kpc. Due to the integrated nature of these quantities, convergence in $V_{\rm max}$ occurs at much higher radii ($\sim$800 pc) than the nominal softening lengths ($\epsilon_{\rm DM} \sim$ 20–40 pc). Distances at which UF circular velocities are measured are well below this convergence radius.

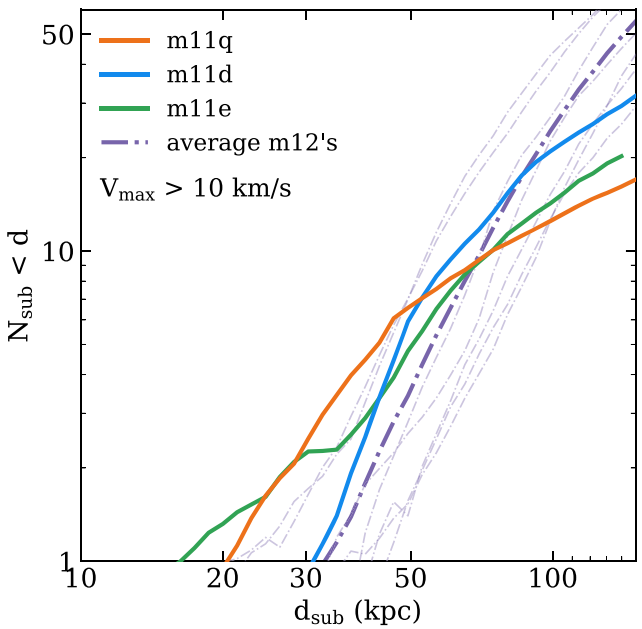

Figure A3. The radial distribution of subhaloes with $V_{\rm max} > 10$ km s^{-1} around three LMC-mass hosts in FIRE (`m11q` – orange; m11d – blue; `m11e` – green) and averaged over seven MW-mass hosts in FIRE (purple dot–dashed line), with all counts averaged over $\sim$1.3 Gyr. We find that two of the three LMC-mass haloes host substructure at significantly smaller distances than the MW-mass haloes, with all hosting more total subhaloes than the average MW-mass halo out to $\sim$60 kpc. The existence of subhaloes at closer distances to the central galaxy for LMC-mass hosts strengthens the plausibility of a detectable subhalo–galaxy interaction for hosts of this scale.

Downloaded from https://academic.oup.com/mnras/article-abstract/489/4/5348/5561484 by University of Texas Libraries user on 02 October 2019

Table A1. Properties of dwarf galaxies near the Milky Way, selected as having either $M_* > 3\times10^4$ $M_\odot$, or begin determined a potential LMC satellite by S17, K18, or this work. All units and coordinates are in the Galactocentric frame. The columns 'possible' and 'confirmed' refer to the LMC association criteria established by Sales et al. (2017, 'S17') and Kallivayalil et al. (2018, 'K18'). Galaxies determined to be consistent with the LMC system by our calculations of angular momenta (listed in Table 3) from *Gaia* DR2 data (Gaia Collaboration 2018) are listed as 'this work.' Any M_* with a star marker (*) was calculated from the visual magnitude listed in K18 (except for Antlia 2, whose M_V was obtained from Torrealba et al. 2018) assuming a mass-to-light ratio of 2. Any V_r with a dagger (†) was converted from its originally tabulated heliocentric value in K18. Numbered superscripts refer to sources. Any row with no superscripts is from McConnachie 2012. A superscript on the name of the galaxy means all properties came from that source. If a property has no superscript but there are others in its row, the nearest superscript to the left is its source.

Name	M_* ($M_\odot$)	l (deg$^\circ$)	b (deg$^\circ$)	D_{MW} (kpc)	D_{LMC} (kpc)	V_{rad} (MW) (km s^{-1})	Possible	Confirmed
Antlia 2	4.30e5^{*,6}	264.9	11.2	124.2	145.4	49.6		
Bootes I	2.90e4	358.5^5	63.3	68.3	98.7	120.4		
Canes Ven. I	2.30e5	74.3	79.8	218	254.1	78		
Carina	3.80e5	264.8^5	−22.5	104	60.8	−13.8		This work
Car2	1.08e4*	270.0^1	−17.1	36.2	25.3	211.4†		K18
Car3	1.56e3*	270.0^1	−16.8	27.8	62.9	51.6†		K18
Cra2	3.26e5*	283.8^2	42.0	116.9	114.5	−79.1†		
Draco	2.90e5	79.2^5	34.3	77.2	125.8	−74.6		
Dra2	2.47e3*	98.3^1	42.9	22.3^2	125.4	−159†	K18	
Eri3	1.08e3^3	274.3^2	−59.6	87.1	48.2		S17	
Fornax	2.00e7	243.84^5	−67.1	146.1	114.5	−38.2		This work
Hercules	3.70e4	28.7	36.9	126	158.5	145		
Hor1	3.92e3^3	270.9^2	−54.9	79.3	38.5	−30.4†		K18, S17
Hor2	1.88e3*	262.5^2	−54.1	79	39.6		S17	
Hyd1	1.30e4*	304.5^1	−16.5	27.6	28.4	−51.4†		K18
Hyd2	1.42e4^3	295.6^2	30.5	125.2	113.5	134.2†	K18	
Leo I	5.50e6	228.1^5	50.1	250.5	263.7	159.6		
Leo II	7.40e5	223.7^5	68.6	231.2	255.2	18.6		
LMC	1.50e9	290.2^5	−32.5	51.8	0.0	43.4		
Phx2	2.25e3^3	323.3^2	−60.2	80.2	51.9		K18, S17	
Ret3^2	2.00e3	273.9	−45.7	92	45.0		S17	
Sag2	2.06e4*	18.9^2	−22.9	60.1	49.6			
Sculptor	2.30e6	318.6^5	−80.2	86.7	65.6	77.0		
Sextans I	4.40e5	250.3	43.7	83.8	94.1	37.7		
SMC	4.60e8	309.4^5	−41.8	66.2	23.2	−4.2		K18, S17
Tuc4^2	2.20e3	313.3	−55.3	45.5	26.6		S17	
Tuc5^2	5.00e2	316.3	−51.9	51.9	28.2		S17	
Ursa Minor	2.90e5	96.5^5	45.6	75	125.4	−72.4		

Note: References: 1 – K18; 2 – S17; 3 – Ferrero et al. (2012); 4 – Koposov et al. (2018); 5 – Gaia Collaboration (2018); 6 – Torrealba et al. (2018).

This paper has been typeset from a TEX/LATEX file prepared by the author.

Downloaded from https://academic.oup.com/mnras/article-abstract/489/4/5348/5561484 by University of Texas Libraries user on 02 October 2019